JOURNAL OF PETROLOGY | VOLUME 54 | NUMBER 3 | PAGES 421–451 | 2013 | doi:10.1093/petrology/egs072

# Adakite-like and Normal Arc Magmas: Distinct Fractionation Paths in the East Serbian Segment of the Balkan–Carpathian Arc

**M. KOLB[1,2]*, A. VON QUADT[1], I. PEYTCHEVA[1,3], C. A. HEINRICH[1], S. J. FOWLER[1] AND V. CVETKOVIĆ[4]**

[1]INSTITUTE OF GEOCHEMISTRY AND PETROLOGY, ETH ZURICH, CLAUSIUSSTRASSE 25, 8092 ZURICH, SWITZERLAND

[2]OMYA DEVELOPMENT AG, BASLERSTRASSE 42, 4665 OFTRINGEN, SWITZERLAND

[3]GEOLOGICAL INSTITUTE, BULGARIAN ACADEMY OF SCIENCES, ACAD. G. BONCHEV ST., 113 SOFIA, BULGARIA

[4]FACULTY OF MINING AND GEOLOGY, UNIVERSITY OF BELGRADE, ĐUŠINA 7, 11000 BELGRADE, SERBIA

**RECEIVED AUGUST 8, 2011; ACCEPTED SEPTEMBER 13, 2012**
**ADVANCE ACCESS PUBLICATION NOVEMBER 12, 2012**

*New age and whole-rock $^{87}Sr/^{86}Sr$ and $^{143}Nd/^{144}Nd$ isotopic data are used to assess petrogenetic and regional geodynamic processes associated with Late Cretaceous subvolcanic intrusions within the sparsely studied Timok Magmatic Complex (TMC) and Ridanj–Krepoljin Zone (RKZ) of eastern Serbia. The TMC and RKZ form part of the Apuseni–Banat–Timok–Srednogorie (ABTS) magmatic belt, a Cu–Au mineralized calc-alkaline magmatic arc related to closure of the Tethys Ocean that extends through Romania, Serbia, and Bulgaria in SE Europe. Zircon ages based on U–Pb laser ablation inductively coupled plasma mass spectrometry supplemented by existing isotope dilution thermal ionization mass spectrometry data respectively range from 89 to 79 Ma and from 76 to 71 Ma for the TMC and RKZ. This age pattern corresponds to cross-arc younging away from the European continent. Adakite-like trace element signatures (Y ≤18 ppm) are linked with samples that extend across the arc. These overlap in space and time with samples that conform to a normal arc differentiation trend. We performed energy-constrained assimilation–fractional crystallization (EC-AFC) modeling of Sr–La–Nd–Yb concentrations and Sr and Nd isotopic data. Results suggest that the two distinct fractionation trends may be explained in terms of a common mantle-derived parental magma but distinct fractionation and assimilation paths in the lower and upper crust. Petrogenesis of the adakite-like magmas is consistent with extensive high-pressure amphibole fractionation in the lower crust followed by ascent and plagioclase-dominant fractionation and assimilation in the upper crust. In contrast, normal arc signatures appear to have evolved exclusively via an upper-crustal differentiation process. Overall, our interpretation supports mantle wedge melting related to weak extension during progressive rollback of a subducting slab.*

KEY WORDS: *arc magmatism; radiogenic isotopes; adakite; EC-AFC; zircon*

## INTRODUCTION

The term 'adakite' is typically used for magmatic rocks with MgO ≤3 wt %, $SiO_2$ ≥56 wt %, $Al_2O_3$ ≥15 wt %, La/Yb ≥20, Sr/Y ≥40 and/or low Y ≤18 ppm (Kay, 1978; Defant & Drummond, 1990; Castillo *et al.*, 1999; Defant & Kepezhinskas, 2001). Calc-alkaline arc rocks that share these distinct trace-element signatures, but have distinct major element concentrations, are known as 'adakite-like'. Adakite petrogenesis has attracted increasing interest and debate in recent years owing to the potential significance of adakitic signatures as tectonomagmatic process indicators. Adakitic signatures are commonly associated with economic porphyry-style and epithermal Cu or Cu–Au–Mo ore deposits (e.g. Oyarzun *et al.*, 2001; Rohrlach & Loucks, 2005; Richards & Kerrich, 2007; Chiaradia, 2009; Chiaradia *et al.*, 2009).

*Corresponding author. E-mail: melanie.kolb@gmx.ch

The characteristic low Y and high Sr concentrations of adakites and adakite-like rocks are generally interpreted in terms of amphibole, garnet, and plagioclase stability. Amphibole or garnet fractionation leads to Y depletion because Y is highly compatible in amphibole and garnet (Kay *et al.*, 1991). Where plagioclase is not stable, Sr becomes enriched in the melt because Sr is compatible in plagioclase. However, the specific nature of the associated petrogenetic processes is debated. Proposed processes include eclogite slab melting and interaction of slab melts with the mantle (Kay, 1978; Defant & Drummond, 1990; Kay *et al.*, 1993; Yogodzinski *et al.*, 1995; Abratis & Wörner, 2001; Kay & Kay, 2002; Jego *et al.*, 2005), melting of thickened mafic lower crust (Atherton & Petford, 1993; Petford & Gallagher, 2001; Bourdon *et al.*, 2002; Kay & Kay, 2002; Chung *et al.*, 2003), and high-pressure fractionation of hydrous magmas with or without melting of the lower crust (Castillo *et al.*, 1999; Rohrlach & Loucks, 2005; Macpherson *et al.*, 2006; Davidson *et al.*, 2007; Chiaradia, 2009; Chiaradia *et al.*, 2009). This last hypothesis may provide a plausible explanation for the relationship between adakite-like magmas and ore deposits, although there is little consensus regarding this topic as yet (Oyarzun *et al.*, 2001; Rabbia *et al.*, 2002; Richards, 2002). High-pressure fractionation of amphibole in the lower crust may be indicative of volatile-enriched parental magmas enhancing the generation of volatile-rich magmas that efficiently transport water, sulfur and ore metals to the upper crust (Hedenquist & Lowenstern, 1994; Burnham, 1979).

In this study, we investigate the origin and evolution of calc-alkaline adakite-like and normal arc magmas that overlap in space and time within the Late Cretaceous Timok Magmatic Complex (TMC) and Ridanj–Krepoljin Zone (RKZ) of eastern Serbia. The TMC and RKZ belong to the 30–70 km wide, >1000 km long Late Cretaceous Apuseni–Banat–Timok–Srednogorie (ABTS) belt that extends across southeastern Europe. The largest porphyry-style and high-sulfidation epithermal Cu–Au deposits of the ABTS belt are spatially and temporally associated with the TMC and RKZ (Mitchell, 1996). Previous geochemical studies on the ABTS magmas have revealed a wide variation (Downes *et al.*, 1995; Jankovic, 1997; Karamata *et al.*, 1997; Banjesevic, 2001; von Quadt *et al.*, 2001, 2005; Ciobanu *et al.*, 2002; Chambefort *et al.*, 2007; Georgiev, 2008; Zimmerman *et al.*, 2008; Georgiev *et al.*, 2009). However, there is little geochemical or petrogenetic information related to the Serbian segment of the ABTS belt.

Here we present new geochronological, whole-rock, major and trace element, and Sr and Nd isotope data for TMC and RKZ subvolcanic rocks. We then focus on modeling the trace element and isotope data using the energy-constrained assimilation–fractional crystallization (EC-AFC) model of Spera & Bohrson (2001). We demonstrate that the adakite-like and normal arc magmas may have been generated from a common source prior to evolution via distinct combinations of lower- and upper-crustal assimilation and fractional crystallization. Variations in age and crustal assimilation processes across the arc form the basis for the development of a new interpretation of the tectonomagmatic evolution of this locally ore-mineralized belt.

## THE ABTS BELT OF SOUTHEASTERN EUROPE

The central Balkan Peninsula of southeastern Europe (Fig. 1) consists of continental fragments that collided prior to the Late Cretaceous closure of the Vardar Ocean (a branch of the former Tethys Ocean): the Dacia Mega-Unit and Tisza Domain European microcontinents, along with the Moesian platform, a promontory of the stable Eurasian plate (Schmid *et al.*, 2008, and references therein; Figs 1 and 2). Vardar subduction occurred beneath the Dacia Mega-Unit, which is subdivided into the Supragetic Unit containing the Serbo-Macedonian Massif, the Getic Unit including the Srednogorie Zone, and the Danubian Unit as part of the Balkan Unit (Schmid *et al.*, 2008; Fig. 2). Associated widespread calc-alkaline magmatism collectively forms the ABTS magmatic belt in eastern Serbia (the target of the present study), the southern Carpathians, Romania, and the Srednogorie zone, Bulgaria (Popov *et al.*, 2002; Figs 1 and 2). Subduction ceased shortly after the end of the Cretaceous (~60 Ma; Karamata & Krstic, 1996; Fügenschuh & Schmid, 2005; Schmid *et al.*, 2008). However, subduction continued throughout the Cenozoic in the Aegean region (Fig. 1) and in the neighboring Alps, leading to dextral translation of the Dacia Mega-Unit (Wilson & Bianchini, 1999) and alternating transpressive and extensional episodes (Marovic *et al.*, 1998; Krstic, 2001) along strike-slip fault zones.

Plate reconstructions and paleomagnetic data show that the Vardar subduction zone was oriented WNW–ESE to east–west in the Late Cretaceous (Patrascu *et al.*, 1994; Neubauer, 2002; Fügenschuh & Schmid, 2005; Schmid *et al.*, 2008). Differential Cenozoic subduction led to clockwise rotation (80°) of the Tisza Domain into the Pannonian Basin, deforming the ABTS belt into its present-day L-shape (Fügenschuh & Schmid, 2005; Ustaszewski *et al.*, 2008; Fig. 1). Rotation acted on the TMC and RKZ segment of eastern Serbia (~30° clockwise), but not on the Srednogorie region in Bulgaria, which remained in an east–west orientation. In Serbia, the Late Cretaceous magmatic complexes are bordered on the west and east by the Eastern Serbo-Macedonian Strike-Slip Zone and the Timok Fault Zone. The Timok Fault Zone shows a north–south dextral offset of ~25–50 km related to the


**Fig. 1.** Schematic overview map of the Alpine–Carpathian arc. Main structural features are shown with dashed lines; the ophiolitic Vardar suture zone of the former Tethys ocean is indicated with a dotted line (modified after de Jonge *et al.*, 1994). Rectangle shows the location of Fig. 2. ABTS belt: Apuseni–Banat–Timok–Srednogorie belt (thick dashed line).

large-scale rotation (Fügenschuh & Schmid, 2005; Figs 2 and 3).

Major element geochemical data and field relations of ABTS belt magmatic rocks have been presented by Popov (1981), Berza *et al.* (1998), Popov *et al.* (2002) and Dupont *et al.* (2002). Published geochronological information consists of numerous K–Ar and Ar–Ar whole-rock and mineral data as well as some high-precision U–Pb zircon and Re–Os ages (von Quadt *et al.*, 2001; Ciobanu *et al.*, 2002; Neubauer, 2002; Stoykov *et al.*, 2004; von Quadt *et al.*, 2005; Chambefort *et al.*, 2007; Georgiev, 2008; Zimmerman *et al.*, 2008; Kouzmanov *et al.*, 2009). An age progression from north to south across the Srednogorie segment of the belt has been interpreted as a consequence of oblique subduction and slab rollback, leading to crustal thinning in the arc and back arc-region in Bulgaria (von Quadt *et al.*, 2005).

## TMC AND RKZ FIELD RELATIONS AND SAMPLING

The Timok Magmatic Complex (TMC) forms a 60 km long × 20 km wide belt of subaerial volcanoclastic rocks pierced by numerous subvolcanic stocks and dikes and some larger plutonic intrusions (Fig. 3). The majority of the intrusive rocks were emplaced at shallow crustal levels, as evidenced by variable phenocryst proportions in microcrystalline matrices, indicating relatively fast magma cooling. The central and southern TMC mainly consists of shallow intrusions (e.g. porphyry stocks and dikes) and volcanoclastic rocks (Karamata *et al.*, 1997). Plutonic intrusions with coarse-grained (≥2 mm) textures reflecting slower cooling are mostly exposed in the western TMC, near Valja Strz (Berza *et al.*, 1998; Fig. 3). Porphyry Cu–Au deposits are exposed within the eastern and northern TMC near the mining towns of Veliki Krivelj, Bor and Majdanpek (Fig. 3). New porphyry Cu–Au prospects were found in the western part of the TMC around the Valja Strz pluton (Avala Resources Ltd.). Published ages of the TMC intrusions range from 90 to 62 Ma (Karamata *et al.*, 1997; Banjesevic, 2001; Banjesevic *et al.*, 2002; Peytcheva *et al.*, 2002; von Quadt *et al.*, 2002, 2003, 2007; Clark & Ullrich, 2004; Banjesevic *et al.*, 2006; Zimmerman *et al.*, 2008).

The Ridanj–Krepoljin Zone (RKZ; Fig. 3) is a poorly delineated 10 km wide belt located some 20 km west of the TMC, consisting of poorly exposed shallow intrusions (Karamata *et al.*, 1997). Some intrusive bodies have caused hydrothermal base metal sulfide replacement and skarn ores in older sedimentary rocks (Berza *et al.*, 1998). More differentiated bodies contain Pb–Zn–Ag (at levels that are not currently economic for mining), and locally, Sb–W mineralization. K–Ar ages are within the range 70–74 Ma (Pecskay *et al.*, 1992).

We collected 27 samples from the TMC and six samples from the RKZ along east–west transects (Fig. 3; Electronic Appendix 1, available for downloading at http://www.petrology.oxfordjournals.org). DUNDEE Precious Metal Inc. (now Avala Resources Ltd.) provided an additional nine borehole samples from the Valja Strz zone of porphyry-style mineralization at the western margin of the TMC. In addition, four samples from the Paleozoic basement were taken, one gneiss and three plutonic rock samples (monzonite, granodiorite, granite; Table 1). All samples from the RKZ represent shallow intrusions, ranging from andesite to rhyolite in composition. Samples from the central TMC, including the Bor area, are sparse owing to poor outcrop exposure. TMC samples include 28 shallowly emplaced porphyritic stocks and dykes and eight plutonic intrusions. The plutonic intrusions are mostly exposed in the western Valja Strz region. One intrusion is present at Majdanpek and another within the southwestern part of the TMC (Fig. 3).

Some samples taken from the porphyry-Cu deposits (Majdanpek, Veliki Krivelj, Valja Strz) show evidence of potassic and propylitic alteration and we have excluded these samples from the geochemical study. Hydrothermal alteration is visible in thin section in some samples. When plotted versus loss on ignition (LOI), elements mobile during hydrothermal alteration (e.g. Ba, Sr, Pb) show enrichment owing to alteration effects for some samples. LOI varies from 0·88 to 6·0 wt %, with most samples plotting between LOI 1·0 and 3·5 wt %. Three samples

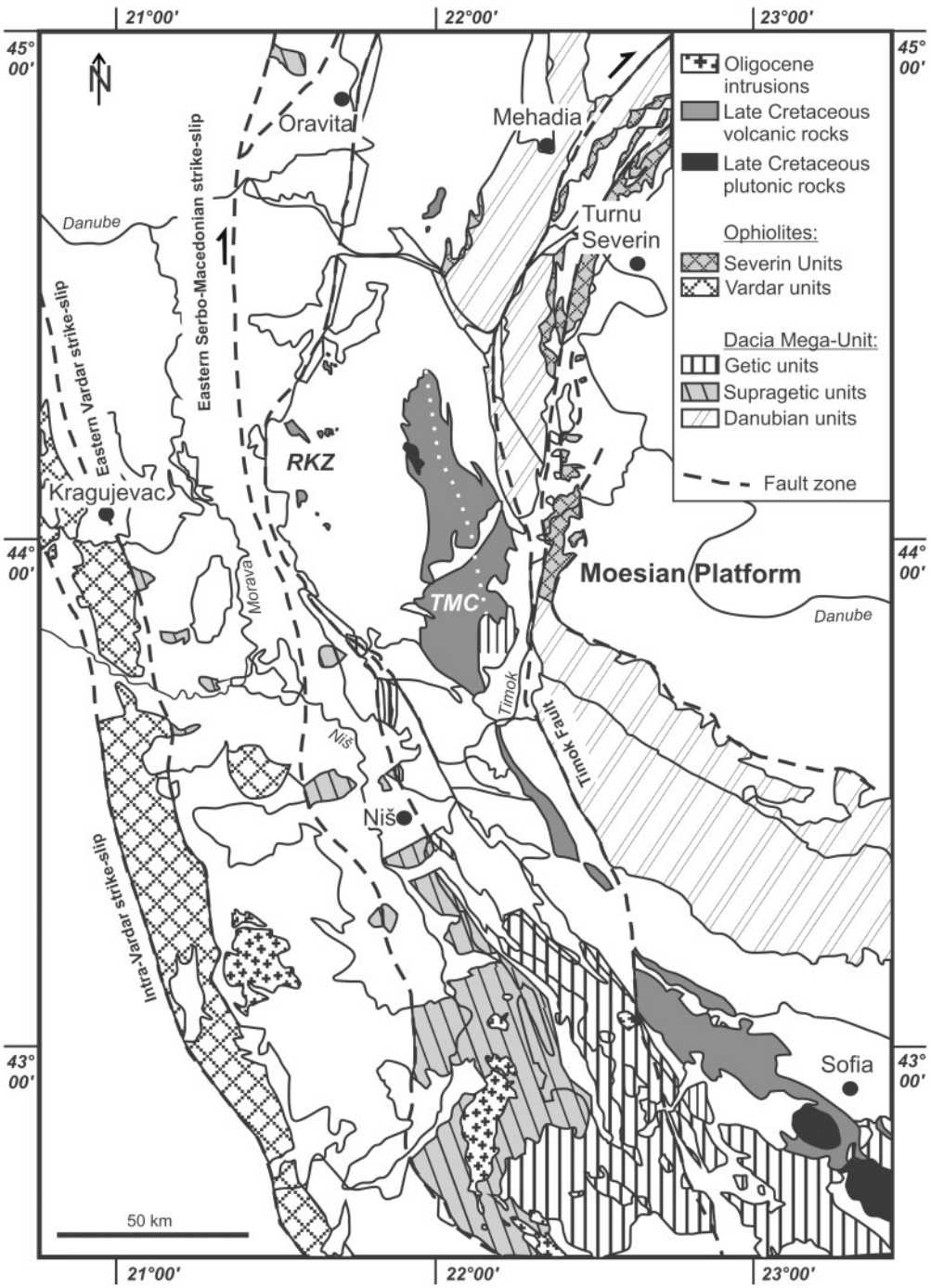


**Fig. 2.** Geological map of eastern Serbia showing the Proterozoic to Mesozoic basement and Cretaceous magmatic rocks of the Timok Magmatic Complex (TMC) and Ridanj–Krepoljin Zone (RKZ) (modified after Kräutner & Krstic, 2003). The white dotted line separates the eastern from the western Timok Magmatic Complex.

showing strong enrichment in fluid-mobile elements (Sr $\geq$1000 ppm, Ba $\geq$1300 ppm, Pb $\geq$50 ppm) and alteration features in thin section were excluded from this study, and one altered sample (MM 34) was used for U–Pb age dating of zircons only.

## ANALYTICAL METHODS

Selected samples were analyzed for major and trace element concentrations plus Sr and Nd isotope ratios. Bulk-rocks were crushed in a tungsten-carbide mill. Major element oxide concentrations were determined by X-ray

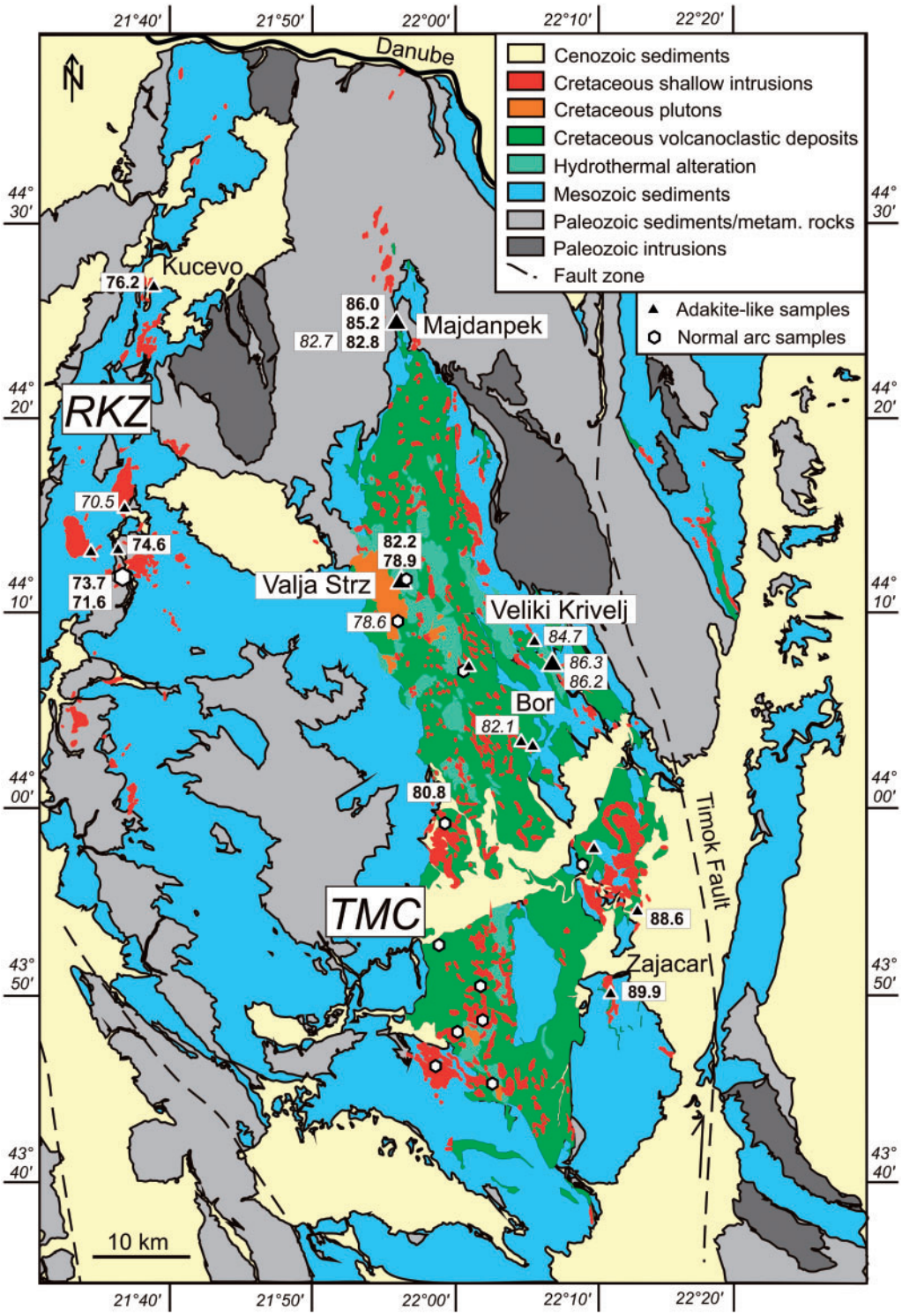


**Fig. 3.** Geological map of the two main belts of calc-alkaline magmatic rocks in eastern Serbia: the Timok Magmatic Complex (TMC) and the Ridanj–Krepoljin Zone (RKZ) (modified after Ciobanu *et al.*, 2002). Numbers in rectangles are U–Pb zircon ages by LA-ICP-MS (bold; this study) and literature U–Pb data (italic; Peytcheva *et al.*, 2002; von Quadt *et al.*, 2002, 2003, 2007). Sampling localities distinguish trace-element data following adakite-like (black triangles) and normal arc samples (white hexagons). Enlarged symbol sizes indicate more than one sample from the same location.

*Table 1: Whole-rock major element (wt %) and trace element (ppm) geochemistry*

| Sample: | AVQ059 | AVQ060 | AVQ 065 | AVQ071 | AVQ072 | AVQ081 | AVQ 218 | AVQ 220 |
|---|---|---|---|---|---|---|---|---|
| Location: | Open pit Veliki Krevelj | 2 km NW of Krevelj | crossroad Bor to Brestovac | North pit Majdanpek | North pit Majdanpek | Open pit Veliki Krevelj | Metownica | Suva Reka |
| Magmatic complex: | E TMC | E TMC | E TMC | E TMC | E TMC | E TMC | E TMC | E TMC |
| Latitude: | 44 07 18 | 44 07 58 | 44 03 44 | 44 25 32·5 | 44 25 32·5 | 44 07 18 | 43 56 06·4 | 43 55 45·3 |
| Longitude: | 22 07 10 | 22 05 55 | 22 05 40 | 21 55 10·8 | 21 55 10·8 | 22 07 10 | 22 08 18·4 | 22 02 02·1 |
| Adakite-like signature: (x) | x | x | x | x | x | x | | x |
| Age (Ma): | *86·17* | *84·66* | *82·05* | *82·73* | Basaltic | *86·29* | Basaltic | |
| Rock type: | Andesite | Andesite | Trachyte | Granodiorite | andesite | Andesite | andesite | Andesite |
| $SiO_2$ | 60·3 | 59·6 | 62·4 | 62·2 | 49·7 | 60·5 | 52·7 | 57·3 |
| $TiO_2$ | 0·46 | 0·52 | 0·44 | 0·49 | 0·68 | 0·45 | 0·97 | 0·64 |
| $Al_2O_3$ | 17·9 | 17·6 | 16·1 | 17·4 | 16·6 | 17·8 | 17·2 | 16·4 |
| FeO | 5·51 | 5·34 | 4·93 | 3·26 | 8·69 | 5·56 | 8·58 | 7·82 |
| MnO | 0·13 | 0·15 | 0·12 | 0·03 | 0·14 | 0·12 | 0·32 | 0·18 |
| MgO | 2·61 | 2·59 | 1·93 | 2·95 | 4·69 | 2·73 | 4·25 | 3·27 |
| CaO | 5·25 | 6·22 | 3·43 | 3·71 | 8·36 | 4·15 | 9·49 | 6·99 |
| $Na_2O$ | 3·95 | 3·25 | 4·64 | 4·44 | 2·44 | 4·13 | 3·16 | 3·11 |
| $K_2O$ | 1·88 | 2·90 | 3·84 | 1·68 | 1·81 | 1·85 | 1·16 | 2·25 |
| $P_2O_5$ | 0·14 | 0·12 | 0·13 | 0·23 | 0·17 | 0·14 | 0·29 | 0·19 |
| LOI | 2·33 | 2·13 | 2·14 | 3·13 | 6·00 | 2·37 | 1·69 | 2·18 |
| Sum | 100·40 | 100·41 | 100·02 | 99·53 | 99·29 | 99·77 | 99·86 | 100·32 |
| Sc | 12·63 | 14·63 | 9·74 | 12·64 | 27·69 | 11·33 | 18·60 | 2·35 |
| V | 158·5 | 171·9 | 130·2 | 97·8 | 273·0 | 150·9 | 194·0 | 19·7 |
| Cr | 10·6 | 9·2 | 106·8 | 9·6 | 93·1 | 9·0 | 42·7 | 25·1 |
| Co | 12·34 | 10·82 | 9·37 | 4·09 | 20·74 | 13·17 | 18·20 | 2·22 |
| Ni | 4·2 | 4·6 | 11·4 | 2·8 | 11·6 | 1·7 | 19·6 | 13·2 |
| Ga | 15·6 | 14·3 | 13·7 | 14·4 | 14·3 | 15·6 | 14·4 | 2·2 |
| Rb | 31·3 | 34·6 | 70·9 | 43·2 | 32·2 | 31·1 | 34·5 | 9·8 |
| Sr | 674 | 458 | 373 | 439 | 708 | 601 | 161 | 203 |
| Y | 11·58 | 11·58 | 11·70 | 14·40 | 13·39 | 10·25 | 19·93 | 8·09 |
| Zr | 65·3 | 54·3 | 87·5 | 80·9 | 51·4 | 63·3 | 91·2 | 77·8 |
| Nb | 3·10 | 4·01 | 4·70 | 5·10 | 2·59 | 3·13 | 4·60 | 2·06 |
| Cs | 0·59 | 0·39 | 0·43 | 1·47 | 2·29 | 0·87 | 4·59 | 0·49 |
| Ba | 364 | 302 | 360 | 192 | 315 | 344 | 399 | 60 |
| Hf | 1·91 | 1·54 | 2·40 | 2·40 | 1·56 | 2·03 | 2·60 | 2·29 |
| Ta | 0·22 | 0·22 | 0·37 | 0·47 | 0·23 | 0·26 | 0·25 | 0·11 |
| Pb | 4·36 | 6·46 | 64·51 | 3·48 | 8·45 | 4·52 | 5·06 | 3·03 |
| Th | 3·18 | 2·10 | 5·79 | 4·57 | 2·31 | 3·18 | 2·77 | 1·71 |
| U | 0·98 | 0·78 | 1·83 | 0·97 | 0·85 | 1·05 | 0·87 | 0·60 |
| La | 11·65 | 7·87 | 16·77 | 8·75 | 10·06 | 11·84 | 13·87 | 7·18 |
| Ce | 23·62 | 17·13 | 30·63 | 20·05 | 22·31 | 24·54 | 28·20 | 12·27 |
| Pr | 2·80 | 2·09 | 3·41 | 2·55 | 3·01 | 2·82 | 3·80 | 1·54 |
| Nd | 11·88 | 8·04 | 13·60 | 11·55 | 12·63 | 11·27 | 17·33 | 6·49 |
| Sm | 2·14 | 1·65 | 2·65 | 2·60 | 2·83 | 2·43 | 3·56 | 1·28 |
| Eu | 0·62 | 0·60 | 0·81 | 0·68 | 0·96 | 0·85 | 1·05 | 0·28 |
| Gd | 1·97 | 1·85 | 2·18 | 2·41 | 2·56 | 2·01 | 3·61 | 1·49 |
| Tb | 0·31 | 0·30 | 0·36 | 0·41 | 0·36 | 0·29 | 0·58 | 0·20 |
| Dy | 2·10 | 2·12 | 2·12 | 2·13 | 2·39 | 2·01 | 3·29 | 1·24 |
| Ho | 0·40 | 0·42 | 0·45 | 0·53 | 0·55 | 0·40 | 0·73 | 0·30 |
| Er | 1·10 | 1·37 | 1·16 | 1·59 | 1·38 | 1·17 | 2·01 | 0·87 |
| Tm | 0·19 | 0·20 | 0·18 | 0·23 | 0·21 | 0·17 | 0·34 | 0·10 |
| Yb | 1·44 | 1·58 | 1·43 | 1·52 | 1·16 | 1·17 | 2·15 | 0·62 |
| Lu | 0·22 | 0·23 | 0·20 | 0·24 | 0·26 | 0·20 | 0·27 | 0·10 |
| Sr/Y | 58·2 | 39·6 | 31·9 | 30·5 | 52·9 | 58·7 | 8·1 | 25·1 |
| La/Yb | 8·1 | 5·0 | 11·7 | 5·8 | 8·7 | 10·1 | 6·4 | 11·6 |

(continued)

*Table 1: Continued*

| Sample: | AVQ059 | AVQ060 | AVQ 065 | AVQ071 | AVQ072 | AVQ081 | AVQ 218 | AVQ 220 |
|---|---|---|---|---|---|---|---|---|
| Location: | Open pit Veliki Krevelj | 2 km NW of Krevelj | crossroad Bor to Brestovac | North pit Majdanpek | North pit Majdanpek | Open pit Veliki Krevelj | Metownica | Suva Reka |
| Magmatic complex: | E TMC | E TMC | E TMC | E TMC | E TMC | E TMC | E TMC | E TMC |
| Latitude: | 44 07 18 | 44 07 58 | 44 03 44 | 44 25 32·5 | 44 25 32·5 | 44 07 18 | 43 56 06·4 | 43 55 45·3 |
| Longitude: | 22 07 10 | 22 05 55 | 22 05 40 | 21 55 10·8 | 21 55 10·8 | 22 07 10 | 22 08 18·4 | 22 02 02·1 |
| Adakite-like signature: (x) | x | x | x | x | x | x | | x |
| Age (Ma): | *86·17* | *84·66* | *82·05* | *82·73* | Basaltic | *86·29* | Basaltic | |
| Rock type: | Andesite | Andesite | Trachyte | Granodiorite | andesite | Andesite | andesite | Andesite |
| $SiO_2$ | 57·2 | 63·0 | 61·1 | 56·8 | 60·2 | 58·3 | 59·6 | 58·5 |
| $TiO_2$ | 0·50 | 0·39 | 0·39 | 0·58 | 0·55 | 0·54 | 0·53 | 0·51 |
| $Al_2O_3$ | 16·1 | 17·5 | 17·4 | 17·8 | 19·3 | 18·1 | 16·6 | 16·7 |
| FeO | 6·03 | 4·09 | 5·41 | 5·87 | 5·77 | 5·83 | 6·58 | 5·84 |
| MnO | 0·12 | 0·09 | 0·08 | 0·13 | 0·12 | 0·13 | 0·11 | 0·07 |
| MgO | 3·29 | 1·65 | 2·16 | 3·29 | 3·02 | 2·76 | 2·77 | 3·29 |
| CaO | 5·71 | 3·71 | 2·98 | 7·82 | 7·48 | 5·40 | 4·76 | 4·75 |
| $Na_2O$ | 2·54 | 4·13 | 3·59 | 3·29 | 3·38 | 4·73 | 3·42 | 2·56 |
| $K_2O$ | 3·28 | 1·72 | 2·25 | 1·43 | 2·51 | 2·24 | 2·97 | 3·40 |
| $P_2O_5$ | 0·16 | 0·14 | 0·17 | 0·18 | 0·18 | 0·21 | 0·19 | 0·20 |
| LOI | 3·95 | 3·19 | 3·56 | 2·45 | -3·10 | 1·56 | 2·47 | 4·15 |
| Sum | 98·95 | 99·57 | 99·05 | 99·68 | 99·37 | 99·70 | 99·98 | 99·91 |
| Sc | 19·87 | 12·43 | 9·36 | 21·14 | 19·89 | 16·75 | 17·33 | 14·66 |
| V | 190·3 | 132·6 | 98·2 | 209·0 | 216·4 | 214·5 | 177·0 | 149·6 |
| Cr | 69·4 | 3·7 | 10·8 | 14·3 | 13·0 | 16·0 | 22·9 | 11·6 |
| Co | 14·15 | 11·72 | 5·02 | 12·14 | 17·52 | 11·64 | 12·55 | 12·46 |
| Ni | 8·6 | 2·8 | 2·3 | 7·0 | 7·5 | 4·0 | 3·0 | 1·9 |
| Ga | 15·0 | 13·4 | 8·8 | 14·8 | 15·6 | 15·3 | 13·9 | 14·1 |
| Rb | 58·9 | 24·1 | 40·4 | 25·2 | 49·1 | 46·3 | 49·1 | 53·0 |
| Sr | 502 | 541 | 307 | 826 | 1188 | 692 | 624 | 409 |
| Y | 14·78 | 8·76 | 9·89 | 14·10 | 13·47 | 15·97 | 15·93 | 16·24 |
| Zr | 75·7 | 63·2 | 48·7 | 64·3 | 68·1 | 79·6 | 78·7 | 82·8 |
| Nb | 4·00 | 2·55 | 3·28 | 2·06 | 1·96 | 2·47 | 5·24 | 5·37 |
| Cs | 2·12 | 0·80 | 1·15 | 0·83 | 0·76 | 0·84 | 1·47 | 1·29 |
| Ba | 471 | 234 | 280 | 305 | 664 | 452 | 565 | 442 |
| Hf | 2·14 | 1·67 | 1·36 | 1·88 | 1·81 | 2·08 | 2·11 | 2·41 |
| Ta | 0·29 | 0·18 | 0·23 | 0·16 | 0·19 | 0·16 | 0·39 | 0·43 |
| Pb | 5·58 | 3·41 | 1·86 | 5·14 | 2·89 | 4·21 | 2·61 | 2·86 |
| Th | 3·88 | 1·79 | 2·29 | 3·77 | 4·14 | 5·23 | 4·33 | 4·43 |
| U | 1·43 | 0·65 | 0·87 | 1·58 | 1·40 | 1·14 | 1·25 | 1·44 |
| La | 13·11 | 6·87 | 8·25 | 14·57 | 14·09 | 19·48 | 12·84 | 14·96 |
| Ce | 26·25 | 14·95 | 17·73 | 30·06 | 28·81 | 33·47 | 24·74 | 28·68 |
| Pr | 3·10 | 1·85 | 2·15 | 3·46 | 3·15 | 4·25 | 3·04 | 3·52 |
| Nd | 12·79 | 7·63 | 9·14 | 14·59 | 14·47 | 17·64 | 12·77 | 14·25 |
| Sm | 2·72 | 1·86 | 2·01 | 3·24 | 2·35 | 3·69 | 2·74 | 3·07 |
| Eu | 0·86 | 0·54 | 0·64 | 1·10 | 0·79 | 1·11 | 0·72 | 0·71 |
| Gd | 2·62 | 1·47 | 1·70 | 2·48 | 2·55 | 3·28 | 3·02 | 3·01 |
| Tb | 0·37 | 0·24 | 0·27 | 0·41 | 0·38 | 0·49 | 0·40 | 0·42 |
| Dy | 2·83 | 1·57 | 1·71 | 2·34 | 2·33 | 2·57 | 2·53 | 2·96 |
| Ho | 0·53 | 0·32 | 0·37 | 0·50 | 0·52 | 0·54 | 0·57 | 0·57 |
| Er | 1·55 | 1·10 | 1·09 | 1·27 | 1·51 | 1·65 | 1·69 | 1·87 |
| Tm | 0·23 | 0·13 | 0·14 | 0·30 | 0·20 | 0·24 | 0·26 | 0·22 |
| Yb | 1·61 | 1·13 | 1·18 | 1·32 | 1·20 | 1·69 | 2·17 | 1·78 |
| Lu | 0·26 | 0·21 | 0·17 | 0·20 | 0·23 | 0·27 | 0·29 | 0·30 |
| Sr/Y | 33·9 | 61·8 | 31·1 | 58·5 | 88·2 | 43·3 | 39·2 | 25·2 |
| La/Yb | 8·1 | 6·1 | 7·0 | 11·0 | 11·8 | 11·5 | 5·9 | 8·4 |

*Table 1: Continued*

| Sample: | MM57 | AVQ067 | AVQ 068 | AVQ076 | AVQ 221 | AVQ 225 | MM28 | MM29 |
|---|---|---|---|---|---|---|---|---|
| Location: | North pit Majdanpek | near Bor lake-Hotel | near Bor lake-Hotel | Crna Reka, Valja Strz | Boljevac | 2 km N of Tanda | Dubrolevac | Dobro Polje |
| Magmatic complex: | E TMC | W TMC | W TMC | W TMC | W TMC | W TMC | W TMC | W TMC |
| Latitude: | 44 25 32·5 | 44 04 55 | 45 04 55 | 44 09 56 | 43 49 13·5 | 43 48 05·3 | 43 48 11·9 | 43 45 27·9 |
| Longitude: | 21 55 10·8 | 22 00 50 | 23 00 50 | 21 56 08 | 21 58 23·8 | 22 00 43·8 | 21 59 57·5 | 22 02 27·9 |
| Adakite-like signature (x): | x | | x | | | | | |
| Age (Ma): | **82·8** | | | *78·60* | | | | |
| Rock type: | Dacite | Basaltic andesite | Andesite | Qz monzo-diorite | Mugearite | Qz monzo-diorite | Latite | Andesite |
| $SiO_2$ | 61·6 | 55·2 | 59·6 | 61·1 | 53·1 | 55·0 | 54·0 | 55·0 |
| $TiO_2$ | 0·49 | 0·62 | 0·51 | 0·56 | 0·64 | 0·66 | 0·74 | 0·72 |
| $Al_2O_3$ | 16·1 | 18·8 | 16·9 | 16·4 | 20·3 | 17·7 | 17·1 | 17·3 |
| FeO | 6·22 | 6·33 | 5·89 | 5·67 | 6·96 | 7·67 | 7·54 | 7·35 |
| MnO | 0·06 | 0·14 | 0·07 | 0·13 | 0·12 | 0·18 | 0·13 | 0·13 |
| MgO | 2·80 | 3·77 | 2·75 | 2·39 | 2·75 | 3·38 | 1·83 | 3·23 |
| CaO | 3·27 | 7·98 | 6·40 | 4·68 | 7·06 | 7·18 | 6·46 | 6·76 |
| $Na_2O$ | 2·90 | 3·50 | 3·57 | 3·54 | 4·20 | 3·63 | 3·94 | 3·40 |
| $K_2O$ | 3·19 | 1·91 | 2·23 | 3·74 | 2·07 | 3·33 | 2·56 | 1·77 |
| $P_2O_5$ | 0·21 | 0·18 | 0·13 | 0·20 | 0·23 | 0·34 | 0·24 | 0·20 |
| LOI | 3·16 | 1·40 | 1·46 | 1·95 | 2·18 | 0·83 | 4·84 | 3·79 |
| Sum | 99·97 | 99·88 | 99·53 | 100·40 | 99·62 | 99·92 | 99·31 | 99·68 |
| Sc | 11·91 | 20·44 | 17·90 | 11·59 | 22·13 | 17·07 | 17·10 | 15·56 |
| V | 136·0 | | 195·7 | 139·3 | 234·7 | 204·7 | 177·3 | 175·0 |
| Cr | 23·2 | 69·5 | 124·1 | 123·0 | 33·0 | 40·2 | 15·5 | 15·1 |
| Co | 13·21 | 21·80 | 14·49 | 12·39 | 19·83 | 19·53 | 19·11 | 19·57 |
| Ni | 3·1 | 14·1 | 15·1 | 11·2 | 14·5 | 11·8 | 12·0 | 8·1 |
| Ga | 14·9 | 16·9 | 13·6 | 14·7 | 16·8 | 16·8 | 15·2 | 14·8 |
| Rb | 64·6 | 47·1 | 35·8 | 130·6 | 46·6 | 102·7 | 48·0 | 39·4 |
| Sr | 396 | 833 | 524 | 614 | 548 | 833 | 606 | 756 |
| Y | 14·80 | 18·36 | 13·94 | 17·51 | 16·67 | 22·33 | 23·60 | 18·82 |
| Zr | 79·0 | 86·0 | 65·7 | 187·5 | 75·3 | 161·7 | 111·2 | 113·6 |
| Nb | 5·00 | 3·99 | 2·87 | 10·04 | 3·53 | 6·63 | 6·17 | 5·56 |
| Cs | 1·18 | 2·53 | 1·42 | 6·29 | 0·52 | 4·54 | 1·22 | 1·86 |
| Ba | 346 | 352 | 264 | 502 | 386 | 596 | 625 | 356 |
| Hf | 2·13 | 2·54 | 1·77 | 5·07 | 1·74 | 4·48 | 2·82 | 3·28 |
| Ta | 0·37 | 0·28 | 0·17 | 1·00 | 0·20 | 0·56 | 0·39 | 0·49 |
| Pb | 3·60 | 141·43 | 25·42 | 26·36 | 7·34 | 20·43 | 11·44 | 12·62 |
| Th | 3·86 | 4·18 | 2·59 | 19·61 | 2·82 | 15·40 | 4·92 | 5·04 |
| U | 1·23 | 1·59 | 1·28 | 4·90 | 1·02 | 3·25 | 1·59 | 1·65 |
| La | 13·05 | 20·30 | 10·47 | 24·36 | 12·17 | 26·30 | 18·93 | 16·94 |
| Ce | 26·44 | 34·17 | 21·75 | 50·09 | 26·07 | 53·17 | 35·86 | 35·51 |
| Pr | 3·18 | 4·17 | 2·69 | 5·71 | 3·24 | 6·55 | 4·63 | 4·45 |
| Nd | 13·03 | 17·91 | 11·43 | 22·20 | 14·67 | 28·57 | 20·63 | 20·71 |
| Sm | 2·68 | 4·29 | 2·73 | 4·33 | 3·41 | 5·96 | 4·52 | 3·54 |
| Eu | 0·72 | 1·33 | 0·86 | 1·25 | 0·98 | 1·36 | 1·29 | 1·18 |
| Gd | 2·75 | 3·22 | 2·63 | 3·82 | 3·43 | 5·49 | 3·18 | 3·20 |
| Tb | 0·41 | 0·57 | 0·43 | 0·64 | 0·43 | 0·66 | 0·62 | 0·55 |
| Dy | 2·44 | 2·98 | 2·49 | 3·17 | 2·93 | 3·83 | 4·12 | 3·65 |
| Ho | 0·54 | 0·74 | 0·49 | 0·70 | 0·63 | 0·81 | 0·81 | 0·58 |
| Er | 1·44 | 1·91 | 1·47 | 2·14 | 1·51 | 2·38 | 2·31 | 1·73 |
| Tm | 0·20 | 0·30 | 0·23 | 0·32 | 0·25 | 0·33 | 0·39 | 0·28 |
| Yb | 1·80 | 2·09 | 1·61 | 2·38 | 1·88 | 2·14 | 2·33 | 1·82 |
| Lu | 0·30 | 0·37 | 0·23 | 0·42 | 0·27 | 0·31 | 0·31 | 0·27 |
| Sr/Y | 26·7 | 45·4 | 37·6 | 35·0 | 32·9 | 37·3 | 25·7 | 40·1 |
| La/Yb | 7·3 | 9·7 | 6·5 | 10·2 | 6·5 | 12·3 | 8·1 | 9·3 |

(continued)

*Table 1: Continued*

| Sample: | MM57 | AVQ067 | AVQ 068 | AVQ076 | AVQ 221 | AVQ 225 | MM28 | MM29 |
|---|---|---|---|---|---|---|---|---|
| Location: | North pit Majdanpek | near Bor lake-Hotel | near Bor lake-Hotel | Crna Reka, Valja Strz | Boljevac | 2 km N of Tanda | Dubrolevac | Dobro Polje |
| Magmatic complex: | E TMC | W TMC | W TMC | W TMC | W TMC | W TMC | W TMC | W TMC |
| Latitude: | 44 25 32·5 | 44 04 55 | 45 04 55 | 44 09 56 | 43 49 13·5 | 43 48 05·3 | 43 48 11·9 | 43 45 27·9 |
| Longitude: | 21 55 10·8 | 22 00 50 | 23 00 50 | 21 56 08 | 21 58 23·8 | 22 00 43·8 | 21 59 57·5 | 22 02 27·9 |
| Adakite-like signature (x): | x | | x | | | | | |
| Age (Ma): | **82·8** | | | *78·60* | | | | |
| Rock type: | Dacite | Basaltic andesite | Andesite | Qz monzo-diorite | Mugearite | Qz monzo-diorite | Latite | Andesite |
| $SiO_2$ | 62·9 | 56·8 | 56·3 | 53·5 | 51·6 | 57·5 | 56·9 | 69·0 |
| $TiO_2$ | 0·35 | 0·84 | 0·79 | 0·78 | 0·83 | 0·43 | 0·55 | 0·25 |
| $Al_2O_3$ | 16·1 | 18·2 | 17·3 | 15·9 | 17·6 | 17·5 | 17·0 | 14·4 |
| FeO | 4·46 | 7·35 | 7·51 | 8·86 | 10·54 | 6·25 | 6·88 | 2·05 |
| MnO | 0·10 | 0·17 | 0·16 | 0·17 | 0·16 | 0·14 | 0·18 | 0·04 |
| MgO | 2·12 | 1·69 | 3·22 | 4·44 | 5·58 | 2·46 | 3·28 | 0·98 |
| CaO | 3·25 | 8·19 | 7·52 | 5·61 | 9·04 | 6·63 | 7·93 | 2·50 |
| $Na_2O$ | 3·97 | 3·34 | 3·47 | 3·89 | 2·21 | 3·62 | 3·37 | 2·50 |
| $K_2O$ | 3·95 | 2·19 | 1·39 | 4·23 | 1·07 | 2·54 | 1·91 | 5·62 |
| $P_2O_5$ | 0·27 | 0·23 | 0·22 | 0·38 | 0·18 | 0·18 | 0·17 | 0·07 |
| LOI | 1·72 | 0·88 | 2·03 | 2·06 | 1·22 | 2·45 | 1·76 | 2·04 |
| Sum | 99·11 | 99·89 | 99·88 | 99·88 | 99·99 | 99·68 | 99·90 | 99·47 |
| Sc | | 20·13 | 19·15 | 18·49 | 36·34 | 11·18 | 21·56 | 5·61 |
| V | | 229·2 | 192·4 | 210·0 | 315·5 | 151·9 | 230·5 | 63·3 |
| Cr | | 22·0 | 20·5 | 59·5 | 35·0 | 4·2 | 5·4 | 8·1 |
| Co | | 25·19 | 15·92 | 23·19 | 58·50 | 35·88 | 72·87 | 138·68 |
| Ni | | 15·5 | 6·1 | 26·0 | 23·8 | 4·2 | 5·1 | 8·4 |
| Ga | | 16·3 | 15·4 | 17·0 | 15·9 | 15·0 | 14·8 | 10·4 |
| Rb | | 53·9 | 47·7 | 126·8 | 28·9 | 64·7 | 69·4 | 117·5 |
| Sr | | 617 | 656 | 941 | 535 | 839 | 994 | 751 |
| Y | | 19·56 | 22·41 | 21·34 | 16·12 | 13·50 | 12·46 | 6·19 |
| Zr | | 86·6 | 114·9 | 155·3 | 43·0 | 58·2 | 48·9 | 89·9 |
| Nb | | 5·40 | 5·86 | 9·05 | 2·75 | 2·54 | 2·47 | 3·49 |
| Cs | | 0·72 | 4·35 | 0·91 | 2·42 | 3·88 | 6·30 | 6·23 |
| Ba | | 370 | 517 | 697 | 91 | 574 | 509 | 999 |
| Hf | | 2·67 | 3·12 | 3·83 | 1·39 | 1·59 | 1·37 | 2·68 |
| Ta | | 0·49 | 0·43 | 0·67 | 0·12 | 0·17 | 0·20 | 1·10 |
| Pb | | 8·36 | 9·88 | 21·85 | 8·06 | 11·45 | 14·28 | 19·49 |
| Th | | 4·49 | 5·06 | 13·27 | 1·41 | 3·70 | 4·42 | 9·24 |
| U | | 1·70 | 1·61 | 3·97 | 0·54 | 1·95 | 1·99 | 3·70 |
| La | | 15·08 | 17·16 | 31·85 | 7·86 | 16·52 | 13·72 | 7·23 |
| Ce | | 30·34 | 35·58 | 66·08 | 19·30 | 34·48 | 30·76 | 13·25 |
| Pr | | 4·04 | 4·23 | 7·97 | 2·56 | 3·76 | 3·53 | 1·36 |
| Nd | | 17·88 | 19·60 | 33·16 | 12·39 | 15·95 | 14·80 | 5·79 |
| Sm | | 4·45 | 4·46 | 7·12 | 3·16 | 3·19 | 2·93 | 1·28 |
| Eu | | 1·05 | 1·23 | 1·65 | 0·95 | 0·95 | 0·89 | 0·37 |
| Gd | | 3·60 | 3·94 | 6·06 | 2·77 | 2·51 | 2·50 | 1·07 |
| Tb | | 0·51 | 0·67 | 0·76 | 0·44 | 0·36 | 0·34 | 0·11 |
| Dy | | 3·68 | 4·08 | 4·13 | 3·07 | 2·43 | 2·19 | 1·00 |
| Ho | | 0·84 | 0·74 | 0·73 | 0·60 | 0·48 | 0·45 | 0·16 |
| Er | | 1·57 | 2·51 | 2·26 | 1·92 | 1·28 | 1·48 | 0·80 |
| Tm | | 0·25 | 0·32 | 0·30 | 0·24 | 0·22 | 0·17 | 0·10 |
| Yb | | 1·82 | 2·55 | 2·20 | 1·74 | 1·35 | 1·34 | 0·63 |
| Lu | | 0·22 | 0·36 | 0·28 | 0·23 | 0·19 | 0·19 | 0·08 |
| Sr/Y | | 31·6 | 29·2 | 44·1 | 33·2 | 62·2 | 79·8 | 121·2 |
| La/Yb | | 8·3 | 6·7 | 14·5 | 4·5 | 12·3 | 10·3 | 11·5 |

*Table 1: Continued*

| Sample: | VS7 | VS11 | VS12 | VS13 | VS14 | AVQ078 | MM39 | MM40 |
|---|---|---|---|---|---|---|---|---|
| Location: | Valja Strz, boreholes | Valja Strz, boreholes | Valja Strz, boreholes | Valja Strz, boreholes | Valja Strz, boreholes | W of Krepoljin | Melanovac | Melanovac |
| Magmatic complex: | W TMC | W TMC | W TMC | W TMC | W TMC | RKZ | RKZ | RKZ |
| Latitude: | 44 12 04 | 44 12 04 | 44 12 04 | 44 12 04 | 44 12 04 | 44 15 45 | 44 11 52·3 | 45 11 52·3 |
| Longitude: | 21 55 45 | 21 55 45 | 21 55 45 | 21 55 45 | 21 55 45 | 21 35 35 | 21 35 54·0 | 22 35 54·0 |
| Adakite-like signature (x): | x | x | | x | x | x | | |
| Age (Ma): | | **82·2** | | | | *70·50* | **73·7** | **71·6** |
| Rock type: | Basaltic andesite | Grano-diorite | Basaltic andesite | Qz monzo-diorite | Grano-diorite | Andesite | Dacite | Andesite |
| $SiO_2$ | 55·6 | 63·8 | 52·8 | 57·4 | 61·1 | 61·9 | 66·8 | 58·8 |
| $TiO_2$ | 0·69 | 0·37 | 0·85 | 0·55 | 0·39 | 0·58 | 0·39 | 0·67 |
| $Al_2O_3$ | 17·5 | 15·2 | 17·8 | 17·5 | 17·4 | 16·3 | 16·5 | 17·7 |
| FeO | 8·41 | 4·72 | 8·76 | 6·78 | 5·41 | 5·23 | 3·16 | 4·97 |
| MnO | 0·12 | 0·07 | 0·17 | 0·15 | 0·08 | 0·11 | 0·06 | 0·08 |
| MgO | 4·46 | 2·00 | 5·76 | 3·16 | 2·16 | 3·00 | 1·90 | 3·70 |
| CaO | 7·01 | 4·47 | 7·47 | 7·48 | 2·98 | 5·11 | 3·85 | 5·90 |
| $Na_2O$ | 2·08 | 2·63 | 2·00 | 3·49 | 3·59 | 3·61 | 4·04 | 4·34 |
| $K_2O$ | 1·74 | 1·65 | 1·34 | 1·80 | 2·25 | 2·32 | 2·01 | 1·71 |
| $P_2O_5$ | 0·22 | 0·11 | 0·20 | 0·18 | 0·17 | 0·25 | 0·16 | 0·39 |
| LOI | 1·86 | 4·55 | 2·91 | 1·24 | 3·56 | 1·37 | 1·34 | 1·64 |
| Sum | 99·61 | 99·58 | 100·09 | 99·77 | 99·05 | 99·76 | 100·13 | 99·97 |
| Sc | 28·64 | 10·45 | 35·79 | 19·51 | 8·97 | 11·20 | 7·67 | 14·62 |
| V | 278·3 | 111·2 | 318·2 | 226·8 | 124·7 | 98·4 | 66·4 | 125·3 |
| Cr | **9·8** | 6·0 | 40·0 | 5·1 | 4·7 | 75·6 | 45·1 | 44·6 |
| Co | 43·74 | 30·20 | 161·85 | 51·37 | 28·68 | 12·00 | 7·65 | 15·67 |
| Ni | 17·4 | 6·3 | 19·3 | 5·4 | 3·7 | 16·0 | 19·1 | 20·4 |
| Ga | 15·0 | 10·8 | 15·8 | 14·0 | 14·7 | 15·9 | 17·2 | 18·8 |
| Rb | 55·8 | 42·8 | 48·0 | 48·1 | 50·5 | 73·9 | 71·4 | 56·7 |
| Sr | 751 | 560 | 544 | 959 | 950 | 655 | 447 | 777 |
| Y | 14·71 | 10·68 | 16·80 | 14·02 | 13·66 | 15·42 | 42·24 | 27·85 |
| Zr | 49·6 | 57·6 | 51·2 | 53·7 | 70·1 | 121·4 | 255·3 | 191·7 |
| Nb | 2·63 | 3·70 | 2·96 | 3·28 | 3·25 | 11·39 | 13·79 | 28·25 |
| Cs | 2·64 | 3·41 | 5·89 | 5·53 | 4·02 | 3·08 | 2·91 | 0·83 |
| Ba | 125 | 445 | 67 | 507 | 621 | 1104 | 1125 | 1297 |
| Hf | 1·44 | 1·69 | 1·69 | 1·61 | 1·93 | 3·32 | 6·00 | 4·26 |
| Ta | 0·22 | 0·33 | 0·27 | 0·67 | 0·22 | 0·73 | 1·06 | 1·39 |
| Pb | 4·89 | 11·29 | 7·38 | 16·74 | 11·35 | 22·16 | 16·61 | 17·61 |
| Th | 2·22 | 3·50 | 1·92 | 4·12 | 4·69 | 11·18 | 7·89 | 12·17 |
| U | 0·84 | 1·36 | 0·94 | 2·57 | 1·75 | 3·37 | 2·40 | 3·36 |
| La | 12·03 | 9·49 | 9·16 | 14·41 | 15·70 | 27·89 | 25·96 | 51·35 |
| Ce | 28·26 | 19·01 | 21·23 | 31·02 | 33·01 | 55·54 | 133·48 | 175·72 |
| Pr | 3·60 | 2·17 | 2·89 | 3·58 | 3·77 | 6·05 | 5·04 | 10·09 |
| Nd | 15·38 | 9·02 | 13·04 | 15·18 | 16·12 | 23·85 | 19·30 | 36·59 |
| Sm | 3·75 | 1·87 | 3·11 | 3·15 | 3·50 | 3·97 | 3·30 | 6·21 |
| Eu | 1·05 | 0·59 | 0·93 | 0·98 | 0·88 | 1·24 | 0·87 | 1·59 |
| Gd | 3·21 | 1·72 | 3·20 | 2·60 | 2·74 | 3·29 | 2·78 | 4·88 |
| Tb | 0·49 | 0·26 | 0·45 | 0·38 | 0·33 | 0·47 | 0·89 | 1·09 |
| Dy | 2·97 | 1·89 | 2·99 | 2·46 | 2·54 | 2·68 | 2·18 | 3·31 |
| Ho | 0·59 | 0·41 | 0·65 | 0·56 | 0·50 | 0·53 | 0·39 | 0·67 |
| Er | 1·59 | 1·19 | 1·91 | 1·48 | 1·48 | 1·59 | 1·11 | 1·45 |
| Tm | 0·21 | 0·17 | 0·27 | 0·23 | 0·22 | 0·26 | 0·17 | 0·23 |
| Yb | 1·43 | 1·37 | 1·58 | 1·68 | 1·55 | 1·66 | 1·09 | 1·58 |
| Lu | 0·23 | 0·24 | 0·28 | 0·24 | 0·26 | 0·24 | 0·15 | 0·29 |
| Sr/Y | 51·0 | 52·4 | 32·4 | 68·4 | 69·6 | 42·5 | 10·6 | 27·9 |
| La/Yb | 8·4 | 6·9 | 5·8 | 8·6 | 10·1 | 16·8 | 23·8 | 32·4 |

(continued)

*Table 1: Continued*

| Sample: | VS7 | VS11 | VS12 | VS13 | VS14 | AVQ078 | MM39 | MM40 |
|---|---|---|---|---|---|---|---|---|
| Location: | Valja Strz, boreholes | Valja Strz, boreholes | Valja Strz, boreholes | Valja Strz, boreholes | Valja Strz, boreholes | W of Krepoljin | Melanovac | Melanovac |
| Magmatic complex: | W TMC | W TMC | W TMC | W TMC | W TMC | RKZ | RKZ | RKZ |
| Latitude: | 44 12 04 | 44 12 04 | 44 12 04 | 44 12 04 | 44 12 04 | 44 15 45 | 44 11 52·3 | 45 11 52·3 |
| Longitude: | 21 55 45 | 21 55 45 | 21 55 45 | 21 55 45 | 21 55 45 | 21 35 35 | 21 35 54·0 | 22 35 54·0 |
| Adakite-like signature (x): | x | x | | x | x | x | | |
| Age (Ma): | | **82·2** | | | | *70·50* | **73·7** | **71·6** |
| Rock type: | Basaltic andesite | Grano-diorite | Basaltic andesite | Qz monzo-diorite | Grano-diorite | Andesite | Dacite | Andesite |
| $SiO_2$ | 62·3 | 69·1 | 63·7 | *65·0* | *76·1* | *52·1* | *62·6* | |
| $TiO_2$ | 0·49 | 0·25 | 0·53 | *0·53* | *0·06* | *0·29* | *0·62* | |
| $Al_2O_3$ | 17·0 | 15·4 | 17·2 | *16·1* | *13·7* | *16·2* | *15·7* | |
| FeO | 4·47 | 2·07 | 4·49 | *4·34* | *0·76* | *2·61* | *5·13* | |
| MnO | 0·08 | 0·05 | 0·13 | *0·02* | *0·02* | *0·13* | *0·09* | |
| MgO | 2·14 | 0·80 | 1·61 | *2·23* | *0·09* | *4·85* | *3·52* | |
| CaO | 5·92 | 3·28 | 4·31 | *1·83* | *0·72* | *5·33* | *4·04* | |
| $Na_2O$ | 3·90 | 4·00 | 3·66 | *4·98* | *3·98* | *5·59* | *3·40* | |
| $K_2O$ | 2·00 | 1·85 | 2·01 | *2·43* | *4·05* | *3·78* | *2·84* | |
| $P_2O_5$ | 0·20 | 0·09 | 0·23 | *0·12* | *0·02* | *0·08* | *0·16* | |
| LOI | 1·49 | 3·20 | 2·23 | *2·36* | *0·71* | *8·79* | *1·35* | |
| Sum | 100·05 | 100·04 | 100·14 | *99·91* | *100·23* | *99·77* | *99·49* | |
| Sc | 11·27 | 2·35 | 8·15 | *8·80* | *3·11* | *6·29* | *15·37* | |
| V | 100·3 | 19·4 | 87·4 | *0·6* | *2·5* | *36·8* | *100·1* | |
| Cr | 50·7 | 15·2 | 18·0 | *29·6* | *17·4* | *54·3* | *145·7* | |
| Co | 10·74 | 3·52 | 9·29 | *13·37* | *0·28* | *5·23* | *12·37* | |
| Ni | 14·3 | 5·4 | 8·8 | *10·0* | *4·0* | *17·9* | *34·5* | |
| Ga | 16·5 | 14·9 | 16·6 | *14·7* | *14·1* | *13·1* | *18·2* | |
| Rb | 68·5 | 67·5 | 64·7 | *55·3* | *120·5* | *101·3* | *122·7* | |
| Sr | 546 | 457 | 666 | *278* | *104* | *129* | *377* | |
| Y | 14·31 | 9·51 | 16·62 | *14·36* | *13·63* | *13·67* | *23·00* | |
| Zr | 117·3 | 128·0 | 126·9 | *121·2* | *51·0* | *121·3* | *198·3* | |
| Nb | 10·41 | 11·69 | 11·73 | *3·42* | *10·21* | *7·72* | *9·83* | |
| Cs | 3·19 | 3·17 | 2·28 | *0·99* | *2·86* | *0·85* | *3·98* | |
| Ba | 641 | 777 | 838 | *237* | *1068* | *434* | *674* | |
| Hf | 3·19 | 3·40 | 3·52 | *3·01* | *2·43* | *4·15* | *5·47* | |
| Ta | 0·79 | 0·96 | 0·89 | *0·26* | *1·42* | *1·19* | *0·81* | |
| Pb | 14·36 | 15·38 | 16·32 | *1·87* | *1·40* | *9·02* | *10·16* | |
| Th | 9·63 | 12·51 | 11·06 | *0·13* | *0·50* | *37·73* | *18·27* | |
| U | 2·66 | 2·61 | 3·24 | *4·52* | *23·38* | *4·30* | *2·95* | |
| La | 26·14 | 32·04 | 30·40 | *8·21* | *23·03* | *22·33* | *29·17* | |
| Ce | 51·09 | 42·61 | 56·50 | *17·49* | *39·83* | *39·87* | *53·50* | |
| Pr | 5·46 | 5·05 | 6·27 | *2·21* | *4·17* | *4·24* | *6·24* | |
| Nd | 20·79 | 17·48 | 24·05 | *9·83* | *16·39* | *16·13* | *24·90* | |
| Sm | 3·42 | 3·24 | 4·57 | *2·30* | *3·10* | *3·05* | *4·45* | |
| Eu | 0·95 | 0·74 | 1·20 | *0·59* | *0·58* | *0·66* | *1·13* | |
| Gd | 3·10 | 2·78 | 3·51 | *2·62* | *3·15* | *2·61* | *3·81* | |
| Tb | 0·44 | 0·32 | 0·46 | *0·38* | *0·43* | *0·33* | *0·67* | |
| Dy | 2·65 | 1·77 | 3·23 | *2·37* | *2·15* | *2·16* | *4·48* | |
| Ho | 0·51 | 0·33 | 0·57 | *0·41* | *0·43* | *0·44* | *0·81* | |
| Er | 1·59 | 1·07 | 2·08 | *1·48* | *1·32* | *1·22* | *2·09* | |
| Tm | 0·19 | 0·12 | 0·20 | *0·19* | *0·18* | *0·24* | *0·38* | |
| Yb | 1·66 | 0·91 | 1·57 | *1·48* | *1·43* | *1·66* | *2·80* | |
| Lu | 0·19 | 0·17 | 0·25 | *0·20* | *0·18* | *0·33* | *0·33* | |
| Sr/Y | 38·1 | 48·1 | 40·1 | | | | | |
| La/Yb | 15·8 | 35·1 | 19·3 | | | | | |

U–Pb ages given are from this paper (bold) and from the literature (italic; Peytcheva *et al.*, 2002; von Quadt *et al.*, 2002, 2003, 2007). LOI, loss on ignition.

fluorescence (XRF) analysis using an Axios PANalytical® wavelength-dispersive (WD)-XRF spectrometer at ETH Zurich. Trace elements and rare earth elements (REE) were determined on freshly broken cross-sections of XRF glass beads at ETH Zurich by laser ablation–inductively coupled plasma–mass spectrometry (LA-ICP-MS) using an Eximer 193 nm system connected to a quadrupole ICP-MS system (Elan6100) with a 60 μm beam diameter and 10 Hz repetition rate. The SRM610 NIST was used as an external standard, and XRF values for CaO were used as an internal standard. Raw data were reduced off-line using SILLS (Guillong *et al.*, 2008). Reported concentrations are the average of three analyses on different domains of a pellet. The analytical reproducibility is <10% for REE and <5% for the other trace elements (Günther *et al.*, 2001). The major and trace element data are reported in Table 1.

Each isotope analysis was performed on 50–100 mg of whole-rock powder. Following digestion in HF and $HNO_3$, Sr and Nd were separated via exchange chromatography on PP columns with Sr-spec, TRU-spec, and Ln-spec resin after Pin *et al.* (1994). Sr and Nd isotopes were loaded on Re filaments and analyzed on Finnigan MAT 262 and Thermo TRITON PLUS mass spectrometers operating in static mode at ETH Zurich. Values for $^{87}Sr/^{86}Sr$ were internally corrected for fractionation using a $^{88}Sr/^{86}Sr$ value of 8·37521. Repeated measurements of the NBS 987 standard gave a mean value of 0·71027 ± 2·6 ppm. $^{143}Nd/^{144}Nd$ values were internally corrected for fractionation using a $^{146}Nd/^{144}Nd$ value of 0·7219. No correction on Sm was performed, owing to good separation during column chemistry. Repeated measurements of the JNd-i standard gave a mean value of 0·512109 ± 1·9 ppm. Age-corrected ($t = 85$ Ma) $^{87}Sr/^{86}Sr$ and $^{143}Nd/^{144}Nd$ values were calculated using Rb, Sr, Sm and Nd concentrations determined by LA-ICP-MS (Table 1).

For U–Pb age determination, zircons were separated from samples, hand-picked, embedded in epoxy resin, and polished. Cathodoluminescence (CL) and back-scattered (BSE) images were collected prior to zircon analysis to identify inherited cores, inclusions and cracks. Measurements were performed in blocks of 20 analyses using the LA-ICP-MS system at ETH Zurich mentioned above. The laser was operated with a 40 μm beam diameter and 10 Hz repetition rate. No $^{204}Pb$ corrections were made, owing to the small count rates. GJ-1 standard (608·5 ± 0·4; Jackson *et al.*, 2004) analysis was performed at the beginning, middle, and end of each block to correct for fractionation. The fractionation correction and results were calculated off-line using GLITTER 4.0 (Macquarie University). For each sample, all concordant ages were used to calculate a mean $^{238}U/^{206}Pb$ age. All ages are given with an error of two standard deviation (2SD) (see von Quadt *et al.*, 2011). Concordia plots, ages, and averaging were processed using ISOPLOT 3.0 (Ludwig, 2003). LA-ICP-MS zircon ages are reported in Electronic Appendix 2.

# RESULTS

## Petrography and geochemical classification

We classified the shallow intrusive rocks based on their whole-rock chemical compositions (after Le Bas *et al.*, 1986; Fig. 4a) and the plutonic rocks ($n = 8$) based on their modal mineral proportions (QAPF classification after Streckeisen, 1976; Fig. 4b). The plutonic and shallow intrusive rocks have similar whole-rock chemistry and are plotted together on the $K_2O$ vs $SiO_2$ diagram (Fig. 4c) of Peccerillo & Taylor (1976). The TMC samples plot within the calc-alkaline, high-K, and shoshonitic fields (Fig. 4c). Data from the RKZ samples are limited to the calc-alkaline field.

The TMC magmatic rocks can be divided into two groups according to geographical location and geology (Figs 2 and 3): (1) eastern TMC, including the easternmost volcanic rocks in the study region and the Majdanpek, Bor, and Veliki Krivelj porphyry Cu deposits; (2) western TMC, including the western and centrally located shallow intrusions and the Valja Strz pluton in the northwestern TMC (Fig. 3). Volcanoclastic rocks are exposed throughout the TMC. In both groups, shallow intrusive compositions range from basaltic andesite/mugearite to dacite/trachyte. One latite porphyry was found in the southwestern TMC. Plutonic rocks are exposed in the Valja Strz region (western TMC; Fig. 3). These comprise quartz monzodiorite and granodiorite to monzogranite. We found only one other granodiorite in the TMC, within the northernmost outcrop of Majdanpek (eastern TMC). Andesite porphyries (52–56 wt % $SiO_2$) are not exposed in the eastern part of the TMC. Shallow intrusive rocks in the RKZ are comparable with those of the TMC and range from andesitic to dacitic.

The shallow intrusive nature of the rocks in both magmatic complexes is reflected in their generally microcrystalline groundmasses with variable phenocryst proportions. Basaltic andesite to latite porphyries contain plagioclase, biotite, and either amphibole or clinopyroxene phenocrysts. Plagioclase is the most common phenocryst in basaltic andesite and intermediate composition samples, followed by either amphibole or clinopyroxene ± biotite. Silica-rich compositions (dacite to rhyolite) mostly contain plagioclase, amphibole, and biotite. In some samples, alkali feldspar and quartz are visible. Apatite is a common accessory mineral in all intermediate and silica-rich samples. Magnetite is present in nearly every sample. For all compositions, the matrix generally consists of plagioclase + magnetite ± clinopyroxene ± biotite. Sometimes amphibole and quartz are present in more evolved

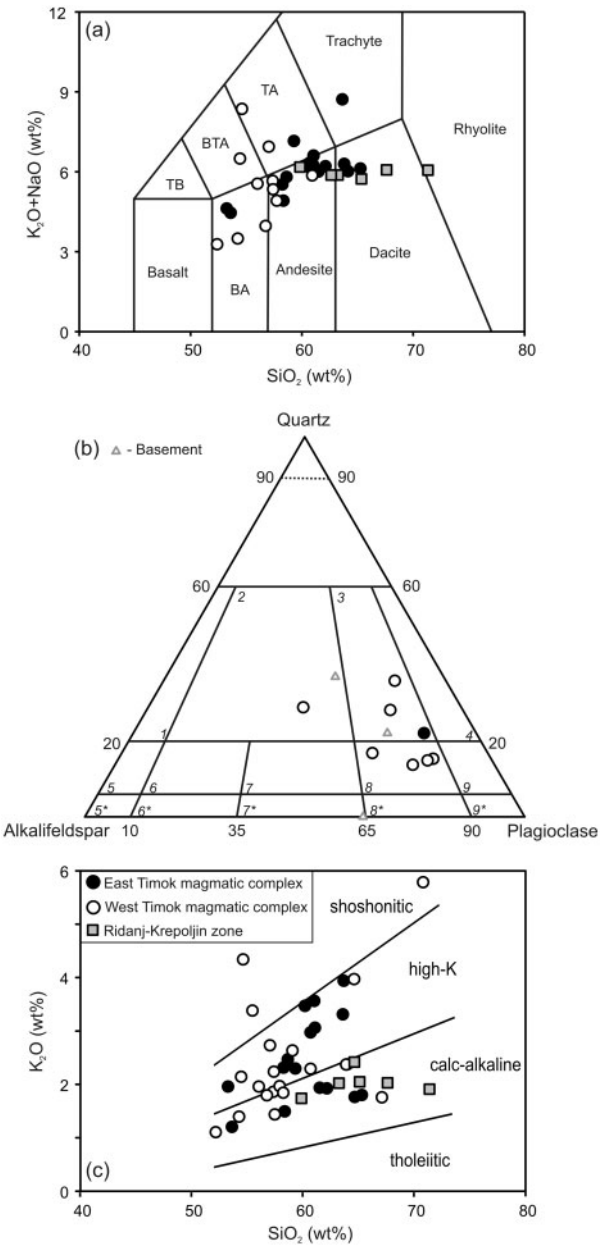


**Fig. 4.** Chemical classifications of shallow intrusive rocks from the TMC and RKZ. (a) Total alkalis vs silica diagram (TAS; modified after Le Bas *et al.*, 1986). (b) Plutonic rocks in the Streckeisen diagram (modified after Streckeisen, 1976). Grey triangles are plutonic basement rocks. (c) The $K_2O$ vs $SiO_2$ classification diagram (Peccerillo & Taylor, 1976) for both shallow intrusive and plutonic rocks. All analyses are recalculated to 100% on a water-free basis. TB, trachybasalt; BTA, basaltic trachyandesite/mugearite; TA, trachyandesite/benmoreite/latite; BA: basaltic andesite. 1, alkali feldspar granite; 2, granite; 3, granodiorite; 4, tonalite; 5, quartz alkali feldspar syenite; 6, quartz syenite; 7, quartz monzonite; 8, quartz monzodiorite/quartz monzogabbro; 9, quartz diorite/quartz gabbro/quartz anorthosite; 5*, alkali feldspar syenite; 6*, syenite; 7*, monzonite; 8*, monzodiorite/monzogabbro; 9*, diorite/gabbro/anorthosite.

samples. Alteration phases, including epidote, chlorite, and calcite, are visible in some thin sections for all compositions. Plagioclase sometimes displays alteration rims of albite or sheet silicates. Amphibole rims can be converted to biotite, whereas biotite crystals commonly show some chlorite alteration. Plutonic rocks contain plagioclase and alkali feldspar as well as amphibole, quartz, and sometimes biotite.

## Major and trace element geochemistry

Table 1 presents major and trace element data for all the studied samples. Variation diagrams for major elements vs $SiO_2$ concentration are shown in Fig. 5. Concentrations of MgO, $Fe_2O_{3total}$, $TiO_2$, and CaO (not shown) are negatively correlated with $SiO_2$, whereas $K_2O$ and $Na_2O$ concentrations show a positive correlation or remain constant. Concentrations of $Al_2O_3$ and $P_2O_5$ are relatively flat at lower $SiO_2$ concentrations, and decrease at $SiO_2$ >55 wt %. Only four samples show enrichment in $P_2O_5$ (>0·25 wt %). $K_2O$ increases slightly with increasing $SiO_2$, up to 60 wt % $SiO_2$. Some samples have elevated $K_2O$ concentrations (>3 wt %), possibly reflecting hydrothermal (potassic) alteration.

Trace element concentrations (e.g. Th, La) generally do not correlate with $SiO_2$ in the western or eastern TMC (Fig. 6). However, all RKZ samples and some data from the western TMC show enrichment in Th and La (Fig. 6a and b). Y concentrations in the TMC and RKZ generally show a negative correlation with $SiO_2$, with the exception of two samples from the RKZ that are enriched in Y (Fig. 6c). There is no clear trend for Sr vs $SiO_2$ in either region (Fig. 6d). REE and trace element patterns normalized to CI-chondrite and enriched mid-ocean ridge basalt (E-MORB) are presented in Fig. 7. Enrichment in light REE (LREE) and relatively flat heavy REE (HREE) patterns are general features of the dataset for the TMC and RKZ. Data from the RKZ generally show LREE enrichment ($La_N/Yb_N$ = 11·3–25·2) compared with those from the TMC ($La_N/Yb_N$ = 3·3–10·4; Figs 6 and 7). All data conform to E-MORB patterns, a typical phenomenon for subduction zone magmas (Fig. 7). Large ion lithophile elements (LILE) such as U, Th and Pb are enriched. The high field strength elements (HFSE) Zr, Hf, Nb and Ta display negative anomalies. These patterns are remarkably similar for both TMC and RKZ, but the relative abundances of most incompatible elements are higher for the RKZ. Most data show slightly negative or positive Eu anomalies (Eu/Eu* 0·6–1·2), but there appears to be no correlation with $SiO_2$.

## Isotope geochemistry

Variations in age-corrected $Sr_i$ and $Nd_i$ isotope ratios (Fig. 8, Table 2) define an array extending between mid-ocean ridge basalts (MORB) and the field of Variscan granitoids (Fig. 8a). Two samples from the eastern TMC,

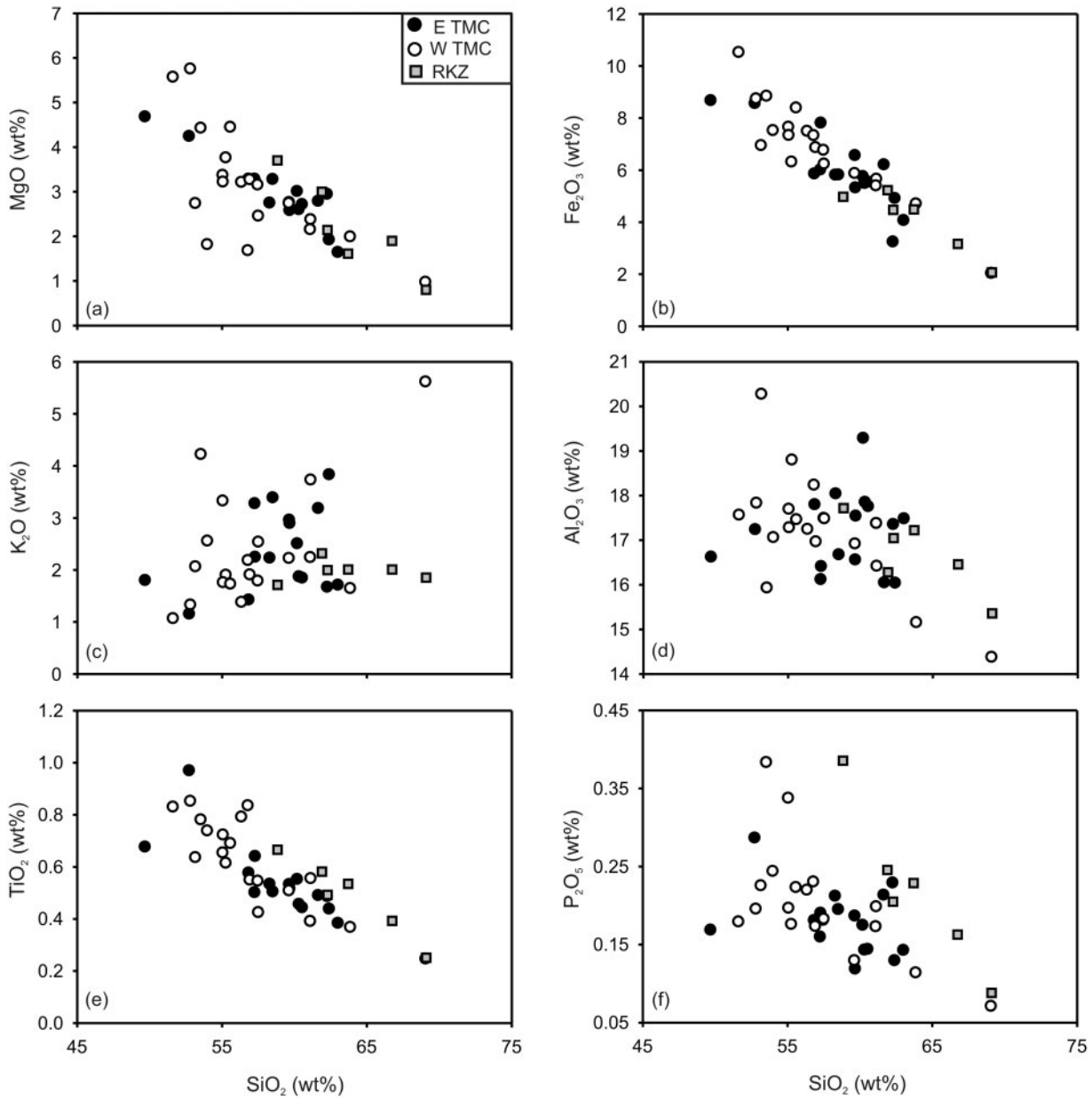


**Fig. 5.** Variation diagrams for major elements vs $SiO_2$: (a) MgO; (b) $Fe_2O_{3total}$; (c), $K_2O$; (d) $Al_2O_3$; (e) $TiO_2$; (f) $P_2O_5$.

respectively dacitic and andesitic in composition, plot in the MORB field. Plots of isotope ratios vs 1/Sr and 1/Nd concentration display no linear correlations (Fig. 8b and c). Some samples overlap with the fields of Variscan granitoids and metamorphic basement rocks (Fig. 8b and c). In general, there is no correlation between Nd–Sr isotopic composition and $SiO_2$ content. The four most primitive samples (lowest $Sr_i$ 0·70339–0·70375 and highest $Nd_i$ 0·512830–0·512716; Fig. 8d and e) are all from the eastern TMC, but they do not have the lowest $SiO_2$ contents in our dataset (58–62 wt % $SiO_2$). Samples from the RKZ are generally more radiogenic than those from the TMC, but one sample is comparable with the TMC in terms of its Nd and Sr isotope composition (Fig. 8a). Data from the eastern and western TMC overlap in Sr and Nd isotope space (Fig. 8a). Based on these data, we infer that contamination by crustal rocks similar to the exposed Variscan basement probably contributed to the geochemical evolution of Cretaceous magmatic rocks in both the TMC and the RKZ. However, magma mixing between basic and acid melts cannot be ruled out.

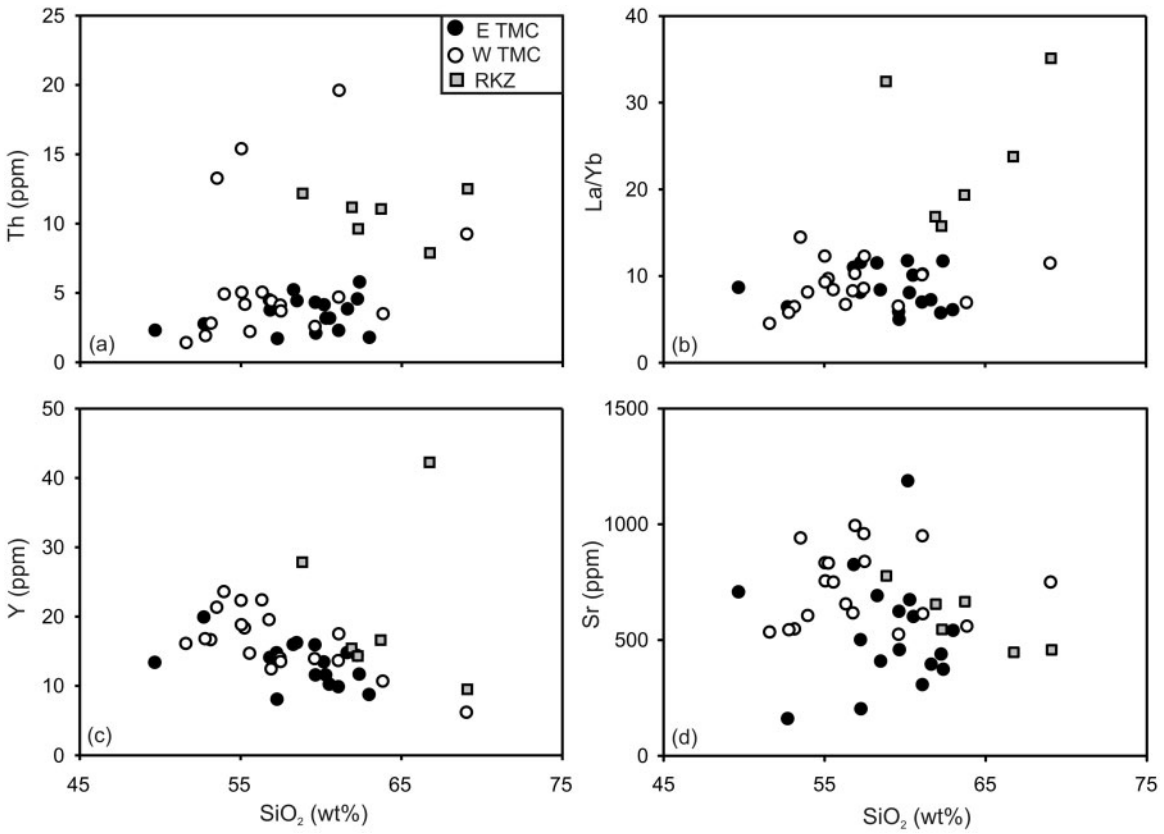


**Fig. 6.** Variation diagrams for trace elements vs $SiO_2$: (a) Th; (b) La/Yb; (c) Y; (d) Sr.

## Geochronology

According to previously published K–Ar age data, magmatism extended from 90 to 62 Ma within the TMC and from 70 to 74 Ma in the RKZ (Jankovic *et al.*, 1981; Pecskay *et al.*, 1992). However, few locations have been dated, and the precision and significance of most ages is questionable. We have obtained new U–Pb ages from 12 zircon-bearing samples (Electronic Appendix 2). These data are displayed in Figs 3 and 9, together with previously published U–Pb ID-TIMS ages, which are in general agreement (Peytcheva *et al.*, 2002; von Quadt *et al.*, 2002, 2003, 2007). Ages from the regions overlap when our cautious LA-ICP-MS errors of 2·5–7% (2SD) are taken into account, but show a general younging from east (TMC) to west (RKZ; Figs 3 and 9) especially if the precise TIMS ages are considered.

Zircon ages decrease towards the west within the TMC, with the oldest ages (89·9 ± 6·0 Ma for MM 47 to 88·6 ± 8·0 Ma for MM 24), from the easternmost part of the TMC (Figs 3 and 9). In the eastern Veliki Krivelj region of the TMC (Fig. 3), ages are between 86·3 and 84·4 Ma (Peytcheva *et al.*, 2002; von Quadt *et al.*, 2002). Two samples from Majdanpek at the northernmost tip of the TMC have ages between 85·2 ± 4·2 and 86·0 ± 7·2 Ma (MM 04, MM 54) and one sample has an age of 82·8 ± 4·4 Ma (MM 57). Older ages seem to be associated with Cu mineralization, whereas one younger age of 82·73 ± 0·03 (AVQ 71; Peytcheva *et al.*, 2002; von Quadt *et al.*, 2002, 2003) postdates mineralization. These data indicate that at least two distinct magmatic events occurred in the Majdanpek region (Figs 3 and 9). Owing to a scarcity of zircons in the central TMC, we obtained ages only in the Valja Strz region near the westernmost boundary. One sample from this region has previously been dated at 78·62 ± 0·44 Ma (von Quadt *et al.*, 2007; Fig. 3). Our new date on a granite dike (78·9 ± 5·2 Ma; sample VS 6a) support the existing date; however, one sample from this area is slightly older (82·2 Ma; VS 11). To the SW, ages are also relatively young, with one sample measuring at 80·8 ± 4·8 Ma (MM 34; Figs 3 and 9).

Ages within the RKZ are markedly younger. Ages generally decrease from 76·2 ± 3·6 Ma (MM 52) in the north to 74·6 ± 4·6 and 73·7 ± 3·4 Ma (MM 41, MM 39) in the south, and to 71·6 ± 6·4 Ma (MM 40) at Krepoljin [in agreement with a TIMS lower intercept age of 70·0 ± 4·1 Ma from von Quadt *et al.* (2007)]. An age gap of a maximum 2·4 Myr may exist between the youngest products of the TMC and the oldest rocks of the RKZ, but this cannot be confirmed owing to large uncertainties associated with the LA-ICP-MS method.

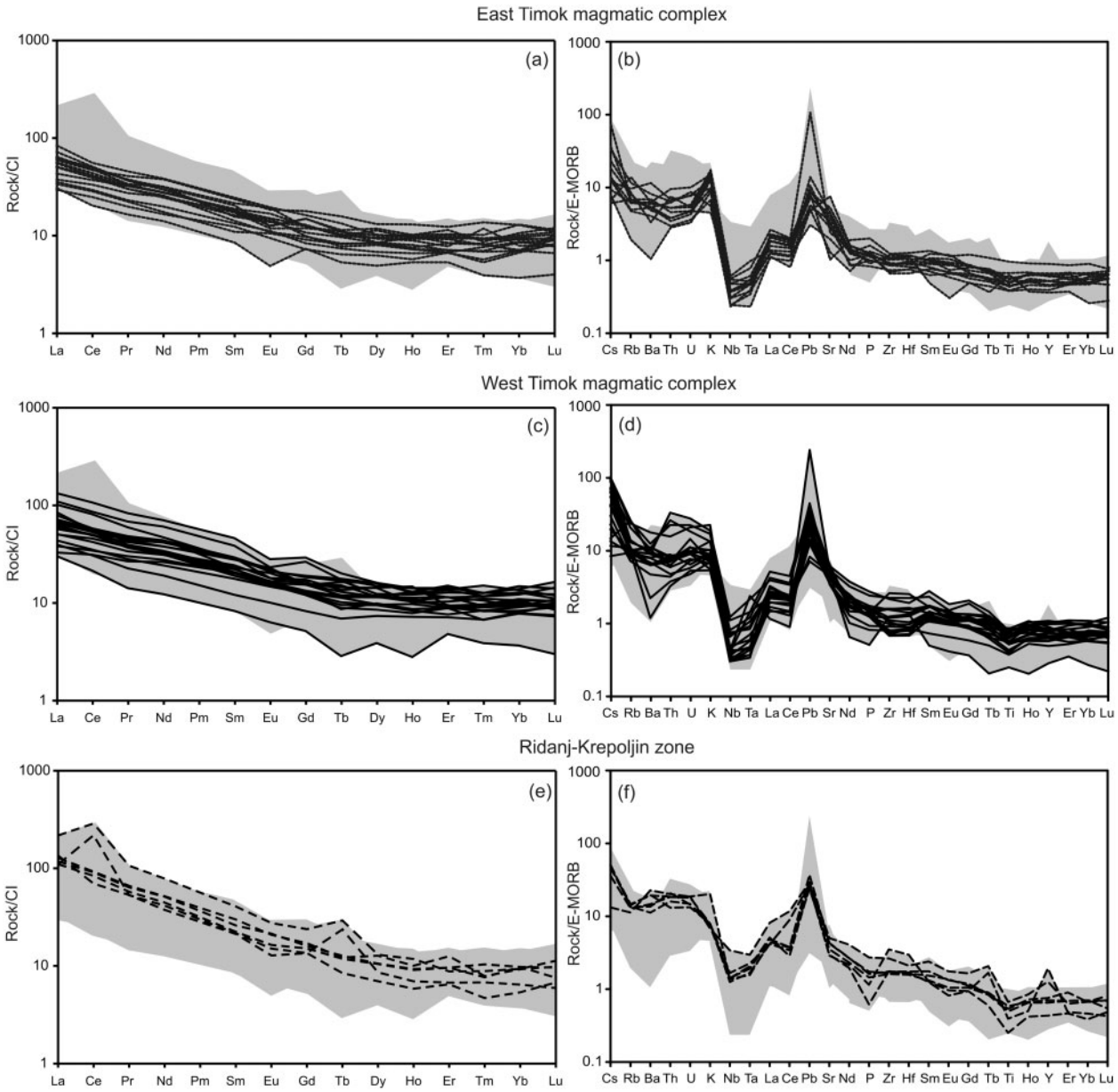


**Fig. 7.** Chondrite-normalized (CI) (a, c, e) and enriched mid-ocean ridge basalt (E-MORB)-normalized (b, d, f) trace element patterns for the TMC and RKZ samples. The grey shaded band represents the overall variation of all samples. Reference values are from Hofmann (1988) and Sun & McDonough (1989).

## PETROGENETIC MODELING OF LOWER- AND UPPER-CRUSTAL DIFFERENTIATION

The Y concentrations and Sr/Y ratios in TMC and RKZ form distinct adakite-like and normal arc trends (Figs 3 and 10). Based on Y concentration and Sr/Y, we subdivide the samples into normal arc and adakite-like, following Castillo *et al*. (1999) and Defant & Kepezhinskas (2001). Adakite-like samples are those with Sr/Y ≥40 and/or Y ≤18 ppm (Fig. 10a). Normal arc samples associated with the TMC have $SiO_2$ contents of 53–58 wt %. Two samples from the RKZ that display Y enrichment (>18 ppm) are also classified as being of normal arc type (Figs 6 and 10, Table 1). All adakite-like samples were collected from the northwestern to eastern part of the TMC and the northern part of the RKZ, whereas the normal arc samples were collected in the south to southwestern portions of both the RKZ and TMC. However, there is no clear spatial distinction between the two regions. We speculate that normal

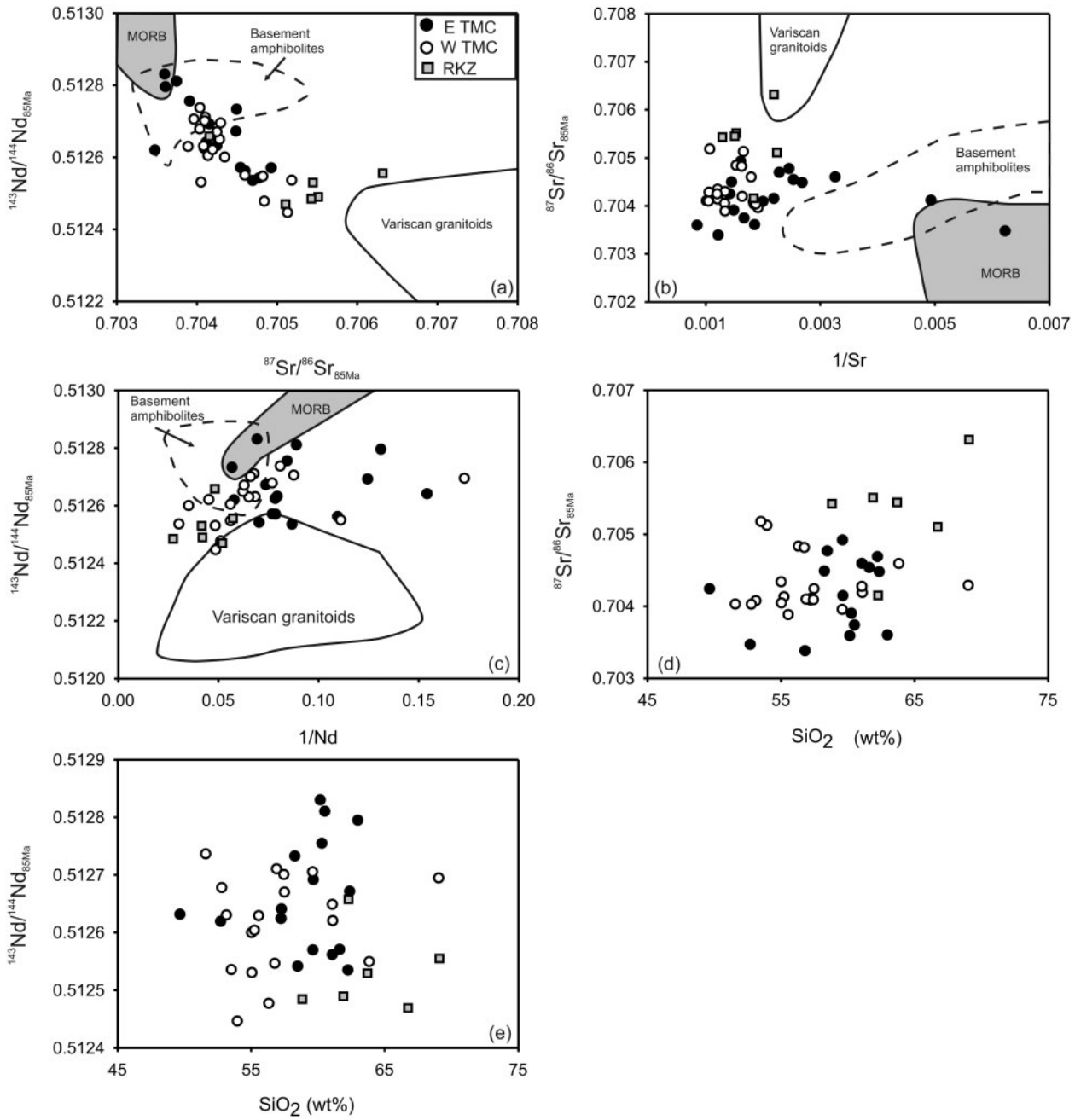


**Fig. 8.** Initial (85 Ma corrected) Sr and Nd isotope ratio plots for the various magmatic areas. (a) $^{87}Sr/^{86}Sr_i$ vs $^{143}Nd/^{144}Nd_i$; (b) $^{87}Sr/^{86}Sr_i$ vs 1/Sr; (c) $^{143}Nd/^{144}Nd_i$ vs 1/Nd; (d) $^{87}Sr/^{86}Sr_i$ vs $SiO_2$; (e) $^{143}Nd/^{144}Nd_i$ vs $SiO_2$. Fields for basement amphibolites and Variscan granitoids are from Liegeois *et al.* (1996) and Duchesne *et al.* (2008), respectively. All isotope ratios are age-corrected to 85 Ma. MORB field data are from Klein (2003) and Stracke *et al.* (2003).

arc and adakite-like trends arose via distinct differentiation processes over an extended time period. We attempt to quantify these processes based on energy-constrained assimilation–fractional crystallization (EC-AFC) modeling. This leads to the conclusion that the TMC–RKZ magmatic province evolved through a combination of lower- and upper-crustal hydrous fractionation of normal arc basaltic andesite with variable contamination by ambient continental crust.

## Observational and published experimental constraints

We consider the origin of this compositional diversity in the light of published petrogenetic hypotheses regarding

*Table 2: Sr and Nd isotopic data for Late Cretaceous magmatic rocks and basement rocks (italic) from TMC and RKZ*

| Sample | Region | Rock type | $^{87}Sr/^{86}Sr$ | $\pm2\sigma_{mean}$ | $^{87}Sr/^{86}Sr_{85Ma}$ | $^{143}Nd/^{144}Nd$ | $\pm2\sigma_{mean}$ | $^{143}Nd/^{144}Nd_{85Ma}$ |
|---|---|---|---|---|---|---|---|---|
| AVQ059 | E TMC | Andesite | 0·704074 | 0·000017 | 0·703908 | 0·512818 | 0·000005 | 0·512755 |
| AVQ060 | E TMC | Andesite | 0·704415 | 0·000016 | 0·704152 | 0·512764 | 0·000008 | 0·512692 |
| AVQ 065 | E TMC | Trachyte | 0·705132 | 0·000018 | 0·704485 | 0·512740 | 0·000005 | 0·512672 |
| AVQ071 | E TMC | Granodiorite | 0·705045 | 0·000011 | 0·704693 | 0·512614 | 0·000004 | 0·512535 |
| AVQ072 | E TMC | Basaltic andesite | 0·704412 | 0·000012 | 0·704248 | 0·512710 | 0·000004 | 0·512632 |
| AVQ081 | E TMC | Andesite | 0·703924 | 0·000008 | 0·703745 | 0·512886 | 0·000002 | 0·512810 |
| AVQ 218 | E TMC | Basaltic andesite | 0·704207 | 0·000002 | 0·703475 | 0·512691 | 0·000007 | 0·512620 |
| AVQ 220 | E TMC | Andesite | 0·704279 | 0·000014 | 0·704114 | 0·512710 | 0·000005 | 0·512641 |
| AVQ 264 | E TMC | Andesite | 0·704490 | 0·000016 | 0·704090 | 0·512699 | 0·000004 | 0·512625 |
| MM01 | E TMC | Dacite | 0·703759 | 0·000019 | 0·703607 | 0·512880 | 0·000002 | 0·512795 |
| MM04 | E TMC | Dacite | 0·705048 | 0·000020 | 0·704600 | 0·512639 | 0·000003 | 0·512562 |
| MM24 | E TMC | Andesite | 0·703493 | 0·000015 | 0·703389 | 0·512648 | 0·000008 | 0·512570 |
| MM38 | E TMC | Andesite | 0·703738 | 0·000009 | 0·703597 | 0·512887 | 0·000001 | 0·512830 |
| MM47 | E TMC | Benmoreite | 0·704723 | 0·000005 | 0·704495 | 0·512806 | 0·000007 | 0·512733 |
| MM54 | E TMC | Andesite | 0·705194 | 0·000004 | 0·704926 | 0·512645 | 0·000005 | 0·512570 |
| MM55 | E TMC | Andesite | 0·705215 | 0·000002 | 0·704773 | 0·512617 | 0·000004 | 0·512542 |
| MM57 | E TMC | Dacite | 0·705099 | 0·000003 | 0·704543 | 0·512643 | 0·000005 | 0·512571 |
| AVQ067 | W TMC | Basaltic andesite | 0·704330 | 0·000016 | 0·704137 | 0·512688 | 0·000014 | 0·512604 |
| AVQ 068 | W TMC | Andesite | 0·704193 | 0·000017 | 0·703961 | 0·512789 | 0·000004 | 0·512705 |
| AVQ076 | W TMC | Qz monzodiorite | 0·705012 | 0·000012 | 0·704195 | 0·512697 | 0·000007 | 0·512621 |
| AVQ 221 | W TMC | Mugearite | 0·704373 | 0·000018 | 0·704083 | 0·512712 | 0·000004 | 0·512630 |
| AVQ 225 | W TMC | Qz monzodiorite | 0·704765 | 0·000012 | 0·704345 | 0·512673 | 0·000008 | 0·512600 |
| MM28 | W TMC | Latite | 0·705307 | 0·000009 | 0·705129 | 0·512523 | 0·000004 | 0·512446 |
| MM29 | W TMC | Andesite | 0·705284 | 0·000002 | 0·704051 | 0·512590 | 0·000006 | 0·512531 |
| MM35 | W TMC | Andesite | 0·705036 | 0·000007 | 0·704821 | 0·512634 | 0·000005 | 0·512547 |
| MM48 | W TMC | Andesite | 0·705088 | 0·000004 | 0·704840 | 0·512557 | 0·000003 | 0·512477 |
| MM50 | W TMC | Latite | 0·705641 | 0·000003 | 0·705182 | 0·512611 | 0·000005 | 0·512536 |
| VS2 | W TMC | Basaltic andesite | 0·704221 | 0·000003 | 0·704036 | 0·512826 | 0·000006 | 0·512737 |
| VS4 | W TMC | Qz monzodiorite | 0·704512 | 0·000003 | 0·704249 | 0·512740 | 0·000003 | 0·512670 |
| VS5 | W TMC | Qz monzodiorite | 0·704341 | 0·000003 | 0·704103 | 0·512780 | 0·000002 | 0·512711 |
| VS6a | W TMC | Monzogranite | 0·704829 | 0·000003 | 0·704295 | 0·512772 | 0·000005 | 0·512695 |
| VS7 | W TMC | Basaltic andesite | 0·704142 | 0·000004 | 0·703888 | 0·512715 | 0·000004 | 0·512630 |
| VS11 | W TMC | Granodiorite | 0·704859 | 0·000002 | 0·704598 | 0·512623 | 0·000001 | 0·512550 |
| VS12 | W TMC | Basaltic andesite | 0·704335 | 0·000007 | 0·704034 | 0·512762 | 0·000002 | 0·512678 |
| VS13 | W TMC | Qz monzodiorite | 0·704268 | 0·000005 | 0·704097 | 0·512773 | 0·000002 | 0·512701 |
| VS14 | W TMC | Granodiorite | 0·704462 | 0·000003 | 0·704281 | 0·512725 | 0·000002 | 0·512649 |
| AVQ078 | RKZ | Andesite | 0·705880 | 0·000015 | 0·705513 | 0·512552 | 0·000009 | 0·512489 |
| MM39 | RKZ | Dacite | 0·705651 | 0·000014 | 0·705106 | 0·512529 | 0·000003 | 0·512469 |
| MM40 | RKZ | Andesite | 0·704405 | 0·000002 | 0·704156 | 0·512717 | 0·000004 | 0·512658 |
| MM41 | RKZ | Dacite | 0·705855 | 0·000018 | 0·705428 | 0·512542 | 0·000003 | 0·512484 |
| MM51 | RKZ | Rhyolite | 0·706820 | 0·000013 | 0·706317 | 0·512620 | 0·000007 | 0·512555 |
| MM52 | RKZ | Dacite | 0·705779 | 0·000005 | 0·705448 | 0·512596 | 0·000006 | 0·512530 |
| *MM56* | *Basement* | *Gneiss* | 0·706711 | 0·000005 | *0·706034* | 0·512636 | 0·000008 | *0·512554* |
| *MM53* | *Basement* | *Granite* | 0·720235 | 0·000007 | *0·716287* | 0·512554 | 0·000012 | *0·512488* |
| *AVQ 223* | *Basement* | *Monzonite* | 0·716584 | 0·000003 | *0·713913* | | | |
| *AVQ 224* | *Basement* | *Granodiorite* | 0·709899 | 0·000003 | *0·708790* | 0·512356 | 0·000003 | *0·512293* |

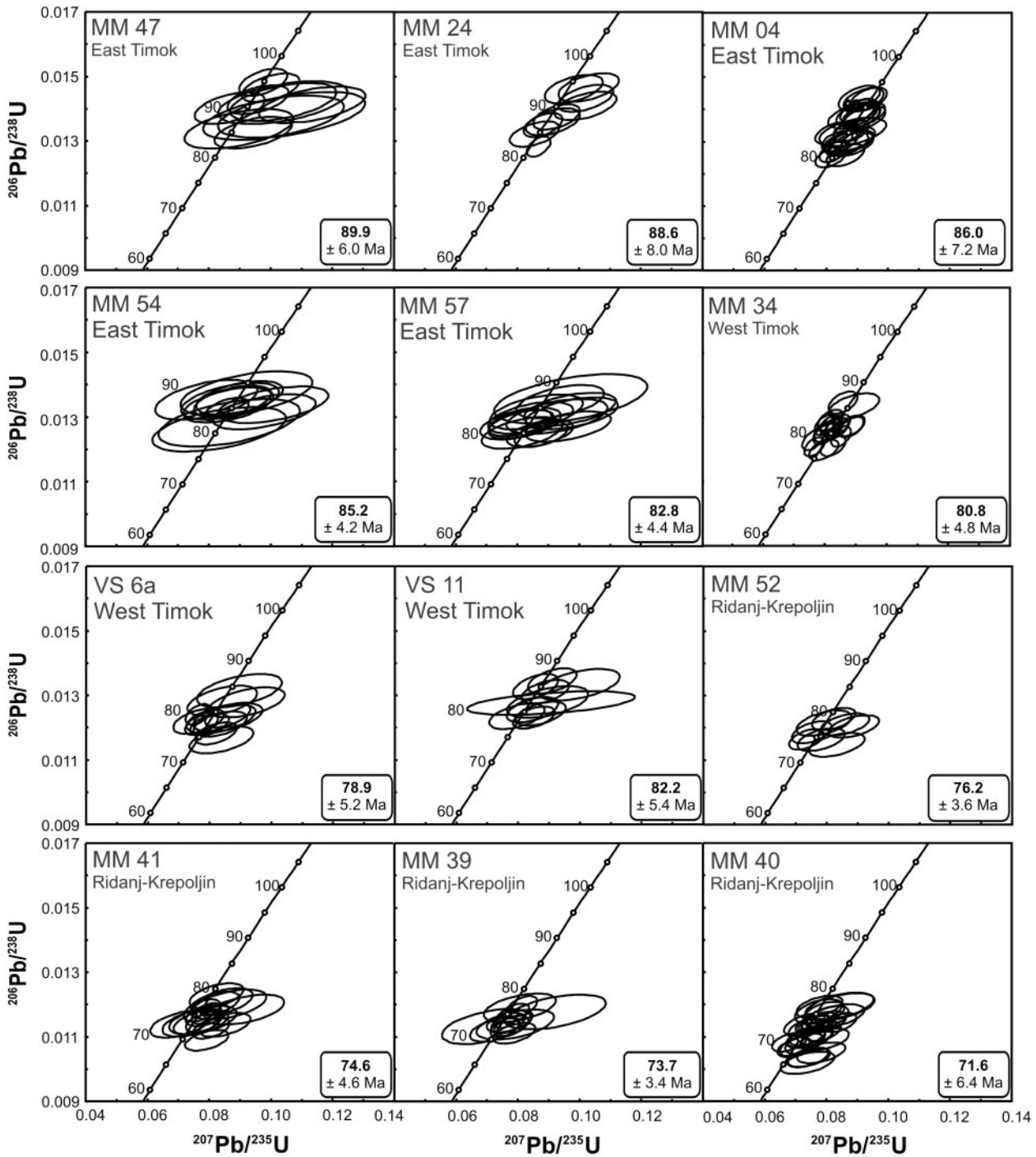


**Fig. 9.** $^{206}Pb/^{238}U$ vs $^{207}Pb/^{235}U$ concordia diagrams. Labeled LA-ICP-MS zircon ages are mean ages ±2 standard deviation (2SD; not standard errors of the mean).

adakite-like magmas associated with Cu deposits worldwide. Previously published hypotheses include partial melting of subducted oceanic crust (e.g. Philippines; Jego *et al.*, 2005), melting of metasomatized mantle rich in garnet and amphibole (e.g. Ecuador; Bourdon *et al.*, 2002), and combined fractionation and assimilation at lower- to upper-crustal conditions (Ecuador; Chiaradia, 2009; Chiaradia *et al.*, 2009). Partial melting of a garnet-rich eclogitic slab would require a hot, and therefore young (≤25 Ma), subducting slab (Defant & Drummond, 1990; Drummond *et al.*, 1996). This scenario is unlikely to have been an important process within the cold subducting Jurassic

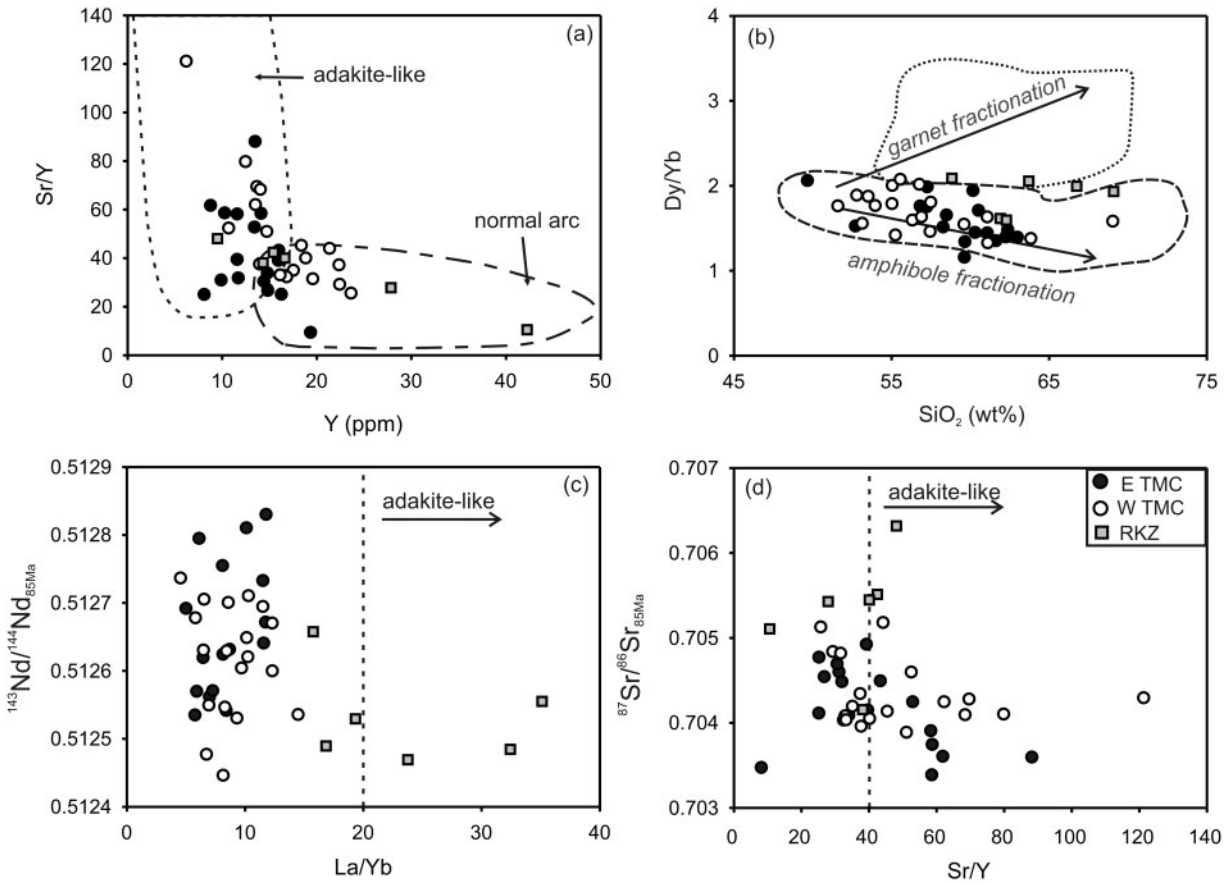


**Fig. 10.** Comparison of adakite-like and normal arc compositions: (a) Sr/Y vs Y; (b) Dy/Yb vs $SiO_2$,; (c) $^{143}Nd/^{144}Nd_i$ vs La/Yb; (d) $^{87}Sr/^{86}Sr_i$ vs Sr/Y. Boundaries for adakite-like and normal arc magma fields (a, c, d) are from Castillo *et al.* (1999). Fields for amphibole and garnet fractionation in (b) are based on literature data (Castillo *et al.*, 1999; Macpherson *et al.*, 2006; Wang *et al.*, 2006; Zhang *et al.*, 2006; Chiaradia, 2009; Hora *et al.*, 2009).

oceanic lithosphere of the Carpathian–Balkan region. Nevertheless, the same effect can be generated by a flat subduction angle. Anomalous heating of the leading edge of the slab during the early stages of flat subduction could lead to slab melting (Gutscher *et al.*, 2000). This cannot be excluded in East Serbia.

In addition, our REE data define slightly U-shaped trends (Fig. 7). Such fractionated middle REE (MREE) and HREE typically indicate high-pressure amphibole fractionation (Castillo *et al.*, 1999; Macpherson *et al.*, 2006; Wang *et al.*, 2006; Zhang *et al.*, 2006; Chiaradia, 2009; Hora *et al.*, 2009), given that the MREE and HREE are preferentially incorporated into amphibole ($D$ Dy>Yb). In contrast, garnet fractionation trends are flatter ($D$ Dy<Yb). Our data show a decrease in Dy/Yb (2·09–1·16) with increasing $SiO_2$, also suggesting amphibole, rather than garnet, fractionation (Fig. 10b; Bourdon *et al.*, 2002). For these reasons we exclude a garnet-rich source (e.g. oceanic crust or garnet-rich metasomatized mantle) as a plausible source for the TMC and RKZ parental melts.

Amphibole fractionation is consistent with lower-crustal depths and high $H_2O$ concentrations in the melt—conditions considered to typify those of magma petrogenesis at subduction zones (Moore & Carmichael, 1998; Davidson *et al.*, 2007). At high pressures (1–2 GPa; ~30–60 km) and high water concentrations (>5 wt % dissolved $H_2O$), amphibole reaches its maximal thermal stability and rank in the crystallization sequence, whereas plagioclase is suppressed (Ulmer, 1988; Alonso-Perez *et al.*, 2009; Maksimov, 2009). Increasing lithostatic pressure at constant dissolved $H_2O$ leads to depolymerization of aluminosilicate melts. Saturation temperatures for minerals that consume higher-order aluminosilicate polymers (e.g. pyroxene and feldspar) are therefore depressed, whereas the thermal stability of hydrous minerals (notably amphibole) increases. The same effect is observed when $H_2O$ increases at constant pressure (Burnham, 1979; Moore & Carmichael, 1998). Amphibole fractionation can also take place at upper-crustal pressures and low water contents, but under such conditions, plagioclase suppression is unlikely.

Plagioclase crystallization depletes Sr in the melt, leading to a normal arc trend with low Sr/Y ≤18 (Fig. 10a). Plagioclase fractionation is also indicated by decreasing CaO and $Al_2O_3$, as well as the presence of negative Eu-anomalies. We infer that elevated Y (≥18 ppm) and positively correlated Y with $SiO_2$ concentration are most probably due to an absence of high-pressure amphibole fractionation in our normal arc samples (Fig. 6). Our REE data thus provide evidence for high-pressure (adakite-like trend) and low-pressure (normal arc trend) fractionation (Fig. 10b). In addition to amphibole and plagioclase fractionation, decreasing MgO, $Fe_2O_{3total}$, and CaO with increasing $SiO_2$ suggest clinopyroxene and magnetite fractionation. Fractionation of MREE and HREE may accompany stabilization of accessory minerals; for example, apatite and titanite (possibly indicated by decreasing $TiO_2$ and $P_2O_5$ with $SiO_2$). However, apatite seems to play an important role only for samples with $SiO_2 \geq 55$ wt % and decreasing $P_2O_5$ contents (Fig. 5f). High Sr/Y values (≥40) can realistically be attained only if plagioclase crystallization is suppressed. Nevertheless, we modelled some scenarios with apatite and titanite, respectively, being the only fractionating phase. The results obtained gave high Sr/Y ratios but do not match for the other trace elements. We have therefore omitted titanite and apatite from the modeling for simplicity.

Crustal contamination, as indicated by elevated $^{87}Sr/^{86}Sr$ and decreasing $^{143}Nd/^{144}Nd$, is variably discernible in both adakite-like and normal arc compositions. All the isotope data trend towards the field of regionally exposed upper-crustal Variscan granitoids (Fig. 8a). Elements enriched in the continental crust (e.g. Th, La) are elevated in the RKZ samples and in some samples from the western TMC. These also serve as an indicator of crustal assimilation (Fig. 6). In addition, Nd isotope ratios in the RKZ samples are correlated negatively with La/Yb (16–35; Fig. 10c), whereas the TMC samples have lower values (La/Yb = 4·5–12·3), possibly indicating a lesser degree of crustal contamination (Fig. 10c). La/Yb is commonly used as a metric for identifying adakite-like rocks. We suggest here that the elevated La/Yb ratios in our dataset may be associated with the addition of La from assimilated continental crust. Adakite-like samples with Sr/Y ≥60 show only relatively minor variations in Sr isotope composition (Fig. 10d). Nevertheless, Sr isotope variations from 0·7035 to 0·7052 indicate that crustal assimilation could have been an important factor in the evolution of these magmas (Fig. 10d). Below we show that these pronounced adakite-like signatures may be associated with assimilation of minor amounts of upper continental crust. Two adakite-like samples from the eastern TMC plot within the MORB field in Sr–Nd isotope space (Fig. 8a), suggesting minimal crustal interaction by these melts. However, the bulk of the adakite-like and normal arc data trend towards elevated Sr and decreased Nd isotope ratios, consistent with combined fractionation and crustal assimilation.

## Composition of end-member components

We modeled the compositional variations by assuming a single parental mantle melt assimilating an upper-crustal composition similar to regionally exposed upper-crustal rocks (Table 3). Mafic rocks (e.g. basaltic andesites) with MgO ≥8 that may represent partial melts of the mantle source are absent in East Serbia. We therefore chose a parental magma with trace element concentrations corresponding to those of a basaltic andesite from the Aleutian Arc (Singer *et al.*, 2007), a similar tectonic setting in which minimal crustal contamination is likely to have occurred (Table 3). Compared with our Sr and Nd isotope data, the Aleutian Arc basaltic andesite has a Sr and Nd isotope composition that is distinctly less enriched ($^{87}Sr/^{86}Sr_i$ = 0·7032, $^{143}Nd/^{144}Nd_i$ = 0·51302), so we have chosen Sr and Nd isotope values similar to those of our least-radiogenic andesite sample MM38 ($^{87}Sr/^{86}Sr_i$ = 0·7036, $^{143}Nd/^{144}Nd_i$ = 0·51285; Table 3). We interpret this sample as being isotopically unmodified following its mantle derivation because it plots within the MORB field (Fig. 8a). Isotope values for our basaltic andesites do not lie within the mantle-derived MORB field (Fig. 8a, d and e), suggesting some crustal contamination.

A dacitic or granodioritic upper-crustal composition was assumed for the assimilant, reflecting the composition of Variscan granitoids (gneiss and granodiorite to granite intrusions; Tables 1 and 2). To augment this sparse dataset from the pre-Alpine (Paleozoic and Phanerozoic) basement in Serbia, we have also considered geochemical data for Variscan granitoids and gneisses of the same Getic basement exposed in Romania (Liegeois *et al.*, 1996; Duchesne *et al.*, 2008). For the modeling, we allowed small variations in the end-member assimilant composition within the range of observational data for granitoid gneisses and intrusions. Amphibolites exposed in the metamorphic basement can be excluded as a significant assimilant source, because their lower $Sr_i$ and higher $Nd_i$ isotopic values do not fall on the correlation trend of the Cretaceous magmatic rocks (Fig. 8a).

## Principle of EC-AFC modeling and input parameters

Previous interpretations of adakite petrogenesis via assimilation and/or fractional crystallization (Castillo *et al.*, 1999; Bourdon *et al.*, 2002; Chiaradia, 2009; Chiaradia *et al.*, 2009) had been based on classic single-step AFC models (e.g. DePaolo, 1981) and trace element indices such as Sr/Y and La/Yb. We use the geochemical dataset from this study in combination with published mineral–melt partition coefficients and an energy-constrained modeling approach (EC-AFC; Spera & Bohrson, 2001) to predict

*Table 3: Parameters and geochemical compositions used for EC-AFC modeling*

| | | | Lower-crustal HP amphibole fractionation; first step scenario 1 and 2 | Upper-crustal fractionation after HP amphibole fractionation; second step scenario 1 and 2 | Upper-crustal fractionation without HP amphibole fractionation; third step scenario 2 |
|---|---|---|---|---|---|
| | *Thermal parameters* | | | | |
| Teq | Equilibration temperature | °C | 990 | 850/920 | 880 |
| Tlm | Magma liquidus temperature | °C | 1320 | 1200 | 1250 |
| $Tm_0$ | Magma initial temperature | °C | 1320 | 1200 | 1250 |
| Tla | Assimilant liquidus temperature | °C | 1100 | 1000 | 1000 |
| $Ta_0$ | Assimilant initial temperature | °C | 700 | 200 | 200 |
| Ts | Solidus temperature | °C | 950 | 850 | 850 |
| cpm | Isobaric specific heat of magma | $J kg^{-1} K^{-1}$ | 1484 | 1484 | 1484 |
| cpa | Isobaric specific heat of assimilant | $J kg^{-1} K^{-1}$ | 1388 | 1375 | 1375 |
| hcry | Crystallization enthalpy | $J kg^{-1}$ | 396000 | 396000 | 396000 |
| hfus | Fusion enthalpy | $J kg^{-1}$ | 354000 | 270000 | 270000 |
| | *Calculation results* | | | | |
| Mm | Mass of melt in magma body | | | 0·507 | 0·248 |
| Ma* | Mass of anatectic melt | | | 0·306 | 0·177 |
| Mc | Mass of cumulates | | | 0·800 | 0·929 |

| | Sr (ppm) | $^{87}Sr/^{86}Sr$ | Nd (ppm) | $^{144}Nd/^{143}Nd$ | La (ppm) | Yb (ppm) | Y (ppm) |
|---|---|---|---|---|---|---|---|
| *Starting composition used for* | | | | | | | |
| Steps 1 and 3 | 450 | 0·7036 | 4·7 | 0·51285 | 3 | 1·1 | 15 |
| Step 2 (end results of step 1) | 807 | 0·7036 | 8·16 | 0·51285 | 6·72 | 1·34 | 6·6 |
| *Assimilant composition used for* | | | | | | | |
| Step 2 | 430 | 0·720 | 10 | 0·51215 | 15 | 0·5 | 12 |
| Step 3 | 300 | 0·709 | 20 | 0·5124 | 17 | 0·7 | 30·5 |

| | Assumed fractionating mineral phases (%) | Partition coefficients (*D*) | | | | | | Assumed fractionating mineral phases (%) | Partition coefficients (*D*) | | | | |
|---|---|---|---|---|---|---|---|---|---|---|---|---|---|
| | | Sr | Nd | La | Yb | Y | | | Sr | Nd | La | Yb | Y |
| *HP amphibole fractionation* | | | | | | | *Dacite composition* | | | | | | |
| HP amphibole | 100 | 0·36 | 0·396 | 0·116 | 0·787 | 1·9 | Clinopyroxene | 3 | 0·5 | 1·4 | 0·3 | 3 | 1·2 |
| *D* bulk | | 0·36 | 0·396 | 0·116 | 0·787 | 1·9 | Amphibole | 20 | 0·6 | 1·2 | 0·26 | 1·31 | 2·46 |
| | | | | | | | Biotite | 2 | 0·31 | 0·339 | 0·28 | 0·44 | 0·6 |
| *Basaltic andesite/andesite composition* | | | | | | | Plagioclase | 50 | 10·7 | 0·19 | 0·2 | 0·11 | 0·51 |
| Clinopyroxene | 10 | 0·12 | 0·4 | 0·11 | 0·8 | 0·72 | Quartz | 25 | 0 | 0 | 0 | 0 | 0 |
| Amphibole | 30 | 0·5 | 0·62 | 0·2 | 1·9 | 1·3 | *D* bulk | | 5·49 | 0·38 | 0·17 | 0·42 | 0·80 |
| Plagioclase | 57 | 2 | 0·074 | 0·14 | 0·03 | 0·066 | | | | | | | |
| Magnetite | 3 | 0·11 | 0·25 | 0·015 | 0·24 | 0·64 | | | | | | | |
| *D* bulk | | 1·31 | 0·28 | 0·15 | 0·67 | 0·52 | | | | | | | |

Trace elements for starting composition 1 and 3 are taken from the Aleutians (Singer *et al.*, 2007). *D* values for EC-AFC calculation are from GERM database; *D* values for high-pressure amphibole are from Martin (1987) and Bottazzi *et al*. (1999).

the evolution of a variety of trace element concentrations and isotope ratios during crustal assimilation and/or fractional crystallization. We base the input parameters for our EC-AFC models on an assumption of high-pressure (lower-crustal) and low-pressure (upper-crustal) processes.

EC-AFC modeling predicts trace element concentrations and isotope compositions within cooling and crystallizing magmas that may potentially heat up and partially melt the surrounding country rocks (Bohrson & Spera, 2001; Spera & Bohrson, 2001). Required input parameters include the initial temperatures of the parent melt and country rocks and experimentally or empirically derived mineral–melt trace element partition coefficients (Table 3). The modeling does not explicitly account for major elements. This would require a full thermodynamic mass-transfer model (e.g. MELTS; Ghiorso & Sack, 1995), for which we would need additional data, notably phenocryst compositions.

Model thermal input parameters are similar to those provided by Bohrson & Spera (2001). Reasonable starting temperatures for the basaltic andesite magma and granodioritic country rocks were chosen based on their compositional range (abbreviations after Bohrson & Spera, 2001; Table 3). We selected country rock initial temperatures ($Ta_0$) consistent with our assumed magma emplacement depths. For the lower-crustal step, we set $Ta_0$ at 700°C (≥20 km; ≥0·8 GPa); for the upper-crustal step, we set $Ta_0$ at 200°C (~6 km; ~0·2 GPa). Local solidus temperatures (Ts) correspond to the lower crust (950°C) and upper crust (850°C).

In each case, the magma initially undergoes fractional crystallization and the country rock heats up. Once the country rock exceeds its solidus temperature (Table 3), it begins to undergo anatexis. All the partial melt generated is considered to be added to the magma instantaneously. The magma continues to cool. Once its temperature corresponds to the solidus (Ts), the calculation ends. The equilibration temperature (Teq) is the third independent variable that affects the chemical and thermal evolution of the magma body. The equilibration temperature is a measure of the extent of thermal interaction between country rock and magma. If Teq > Ts, the calculation ends when the equilibration temperature is attained. High equilibration temperature implies higher effective heat conduction into the country rocks, thus increasing the mass of anatectic melt, whereas lower equilibration temperature generates a smaller mass of anatectic melt owing to smaller heat transfer to the country rocks. On the other hand, the melt quantity remaining in the magma body is reduced by lower Teq as a result of increasing fractionation, thus leading to a greater compositional effect upon the resulting mixed melt (Spera & Bohrson, 2001).

We selected for our modeling two LREE (La and Nd), one HREE (Yb), Sr and Y. At the same time, we calculated the resulting Sr and Nd isotope variations. High-pressure amphibole was assumed to be the sole mineral phase crystallizing at lower-crustal conditions, utilizing appropriate *D* values (Table 3). For upper-crustal fractionation we assumed a stable phase assemblage of dominantly plagioclase (57%), a smaller fraction of low-pressure amphibole (~30%, with *D* chosen to correspond to normal magmatic amphibole; Table 3) and clinopyroxene (~10%), and minor magnetite (3%). All values for mineral–melt trace element partition coefficients (*D*) were taken from the GERM database (http://earthref.org/KDD/; Table 3). Bulk *D* values for the crustal assimilant were calculated in the same way, assuming a dacitic composition (Table 3).

## Scenario 1: sequential lower- and upper-crustal assimilation and fractional crystallization

Here we investigate whether normal arc and adakite-like compositions may all be accounted for in terms of derivation from a single parental magma evolving via successive assimilation and fractional crystallization in the lower and upper crust.

An initial episode dominated by lower-crustal amphibole fractionation may account for the high Sr/Y (≥40) adakite-like portion of our dataset (Figs 10a and 11a). Associated Sr isotope variation is small (Fig. 10d), suggesting that the extent of crustal incorporation was minor. Accordingly, our lower-crustal model results are consistent with an initial phase in which fractional crystallization dominates (light blue dashed arrow; Fig. 11), followed by assimilation (dark blue dashed arrow; Fig. 11). Model results for Sr/Y vs Y are consistent with the adakite-like data (Fig. 11a), but the predicted REE variations do not coincide with the observed data (Fig. 11b and d). Therefore, we hypothesized a second step in which melt generated via an initial episode of lower-crustal fractionation subsequently evolved at conditions corresponding to the shallow crust (~6 km depth; Fig. 11). Predicted element concentration data from the conclusion of the initial (lower-crustal) step form the starting composition for the subsequent (upper-crustal) step. For an equilibration temperature of 850°C, predicted Y contents as high as those observed in the normal arc samples (up to 42 ppm; Figs 10a and 11a) can be achieved, but the best-fit model predictions coincide poorly with other trace elements and particularly the Nd and Sr isotope data (grey arrows; Fig. 11). We therefore conclude that the normal arc samples were not derived from a parental magma that, like the adakite-like samples, first underwent high-pressure amphibole fractionation.

## Scenario 2: concurrent lower- and/or upper-crustal assimilation and fractional crystallization

As an alternative scenario, we considered whether our data may reflect derivation from a common parental melt,

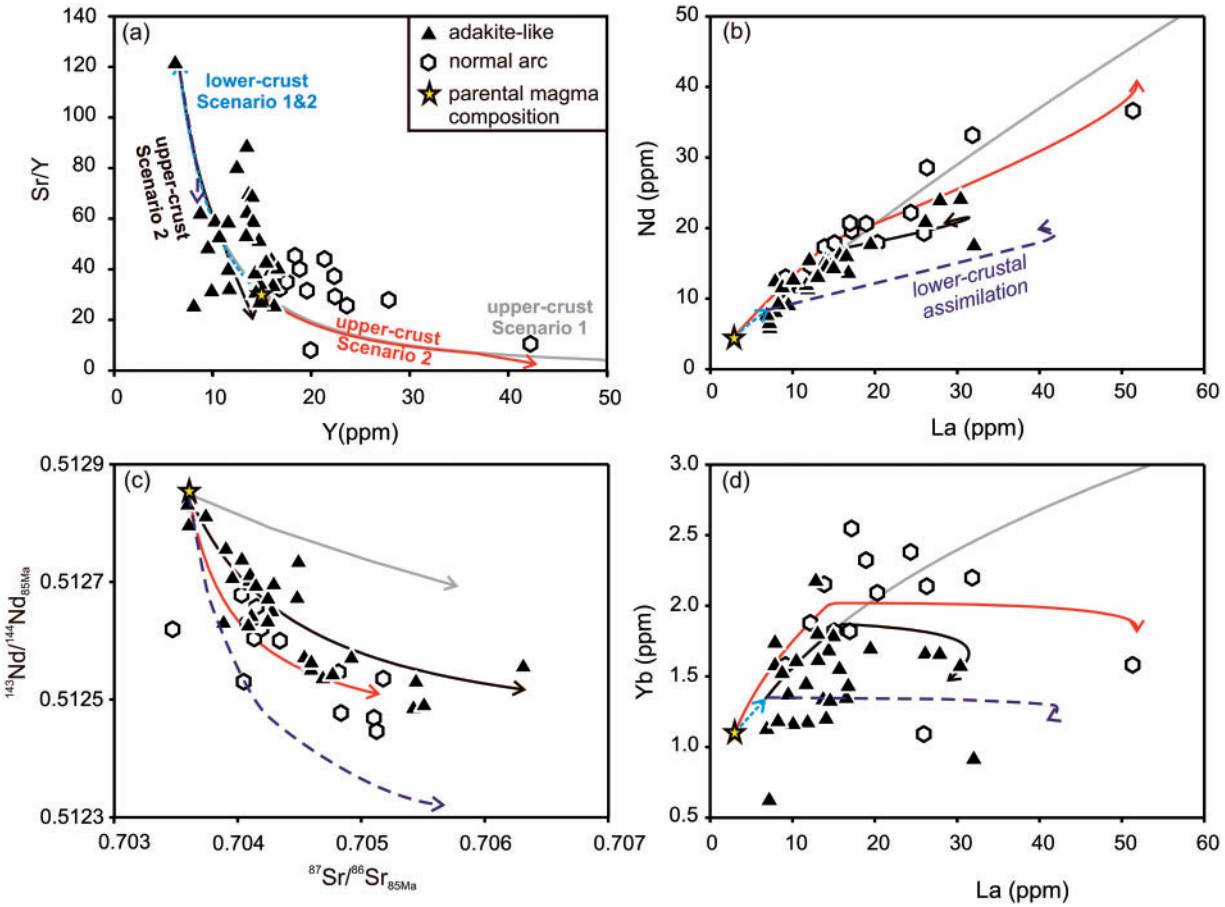


**Fig. 11.** Results from the EC-AFC modeling for Scenarios 1 and 2 described in text. (a) Sr/Y vs Y; (b) Nd vs La; (c) $^{143}Nd/^{144}Nd_i$ vs $^{87}Sr/^{86}Sr_i$; (d) Yb vs La. The yellow star indicates the parental magma composition; light blue dashed arrow, lower-crustal modeling step with high-pressure amphibole fractionation for scenario 1 and 2; dark blue dashed arrow, lower-crustal assimilation starting after extensive high-pressure amphibole fractionation; grey arrow, second upper-crustal modeling step scenario 1; black arrow, second upper-crustal modeling step scenario 2; red arrow, third upper-crustal modeling step 3 in scenario 2.

from which some magma batches were directly injected into the upper crust, whereas other magma batches evolved as proposed for Scenario 1 (i.e. via extensive successive lower- and upper-crustal assimilation and fractional crystallization).

This test involves three distinct EC-AFC calculations. The first two steps are aimed at accounting for adakite-like isotope and REE compositions. Input parameters for the first calculation correspond to lower-crustal conditions; the second calculation uses thermal input parameters based on upper-crustal conditions and geochemical inputs that correspond to the end of the first calculation. The first calculation generates adakite-like Sr–Y trends (blue dashed arrows; Fig. 11) and is identical to that of Scenario 1 (high-pressure amphibole fractionation at lower-crustal conditions). For the second calculation, similar to the second step in Scenario 1, we hypothesize crystallization of an assemblage dominated by plagioclase, low-pressure amphibole, pyroxene and magnetite. For an equilibration temperature adjusted to 920°C (Table 3), the calculated trends coincide well with the adakite-like dataset (black arrows; Fig. 11b–d). The third calculation is aimed at modeling the normal arc data. We use the same parental magma composition as for the other calculations and the same mineral phases and upper-crustal thermal parameters as for step 2 of this scenario. The magma starting temperature was chosen as 1250°C and the equilibration temperature was fixed at 880°C. This scenario is consistent with direct injection of parental magma into cooler upper crust. The mass of anatectic melt Ma* is about half of the mass generated compared with the second calculation here, in which adakite-like melts evolving in the upper crust first resided in the lower crust (Table 3). These results best fit the REE, Sr and Y concentration data and Sr and Nd isotope values for the normal-arc samples (red arrows; Fig. 11).

### Summary of modeling results

Although our hypotheses, selected input parameters, and the EC-AFC model itself, like all computational models, do not account for the wide degree of complexity observed in nature, we draw the following general conclusions. Adakite-like and normal arc melts may have been derived from a common parental magma similar to a mantle-derived hydrous basaltic andesite. Evolution of adakite-like melts probably involved extensive high-pressure amphibole crystallization at lower-crustal conditions followed by plagioclase-dominated upper-crustal fractionation and assimilation of broadly granodioritic Variscan basement. Evolution of normal arc melts, in contrast, probably did not involve high-pressure amphibole fractionation; these melts evolved within the upper crust by combined fractionation and assimilation. Minor assimilation of isotopically similar lower crust for the normal arc melts cannot be excluded given the simplifications of the modeling. Some variation in assimilant composition is likely, given that the coeval adakite-like and normal-arc melts overlap geographically in some locations. Therefore, we now turn to discussing regional variations in emplacement age and magma composition.

## TECTONO-MAGMATIC INTERPRETATION

Here we consider the relationship between melt geochemical variation, emplacement age, and sample location as a basis for interpreting the spatio-temporal evolution of the RKZ and TMC magmatic systems. From this we derive a lithosphere-scale tectonic model for the Balkan–Carpathian active continental margin during Late Cretaceous times.

### Across-arc geochemical variations

In the light of the predominantly NNW–SSE extension of the volcanic complexes and all major tectonic boundaries within the orogen, we projected the measured emplacement ages, selected geochemical parameters, and isotopic ratios onto a cross-section extending from WSW (Ridanj–Krepoljin) to ENE (West Timok; Fig. 12, labeled as distance from the starting point MM 51).

Emplacement ages, shown in Fig. 12a, display a distinct younging from the eastern TMC (89 Ma) to the western TMC (78 Ma), and to the youngest ages between 76 and 71 Ma measured on RKZ samples. Figure 12b shows once again that adakite-like magmas were emplaced throughout the TMC and RKZ and for the entire duration of magmatism in both complexes. Even though many adakite-like magmatic complexes are barren, all areas containing major economic copper deposits (e.g. Majdanpek, Veliki Krivelj and Valja Strz) are associated with adakite-like porphyry intrusions. This probably reflects the hydrous nature of the magmas, favoring amphibole over plagioclase fractionation. High magmatic volatile contents and extensive magmatic differentiation processes are the key to the formation of metalliferous hydrothermal magmatic fluids. These fluids, forming the ore deposits, are exsolved during the late stages of magmatic evolution after the emplacement of the magmas in the upper crust (e.g. Hedenquist & Lowenstern, 1994).

Trace element signatures and isotopic indicators of crustal contamination also vary from the western TMC to the RKZ (Figs 6–8). Concentrations of elements enriched in the crust (e.g. Th, Ba, La) are highest in the RKZ and some samples of the eastern TMC (Figs 6 and 7), consistent with Sr- and Nd-isotope constraints. Samples with the most depleted Sr and Nd isotope compositons, overlapping the MORB field, are associated with the beginning of volcanism at 89 Ma in the easternmost part of the TMC ($^{87}Sr/^{86}Sr_i$ ~0·7034; $^{143}Nd/^{144}Nd_i$ up to 0·5128; Fig. 12c and d). There is a general trend of increasing $^{87}Sr/^{86}Sr_i$ (to a maximum of 0·7049) and decreasing $^{143}Nd/^{144}Nd_i$ (to a minimum of 0·51263) up to 82 Ma. Between 82 and 78 Ma, Sr isotopic values decrease (maximum 0·7046; Valja Strz region) and Nd isotope values increase (maximum 0·51273; Valja Strz region). We interpret this pattern as indicating a short and localized period of asthenospheric input (continuous-line arrows in Fig. 12c and d), after which the Sr and Nd isotope signatures indicate a return to greater crustal contamination. Magmas in the RKZ reach the maximum degree of crustal contamination and those from the easternmost TMC are the most dominated by mantle-like values; however, fairly primitive mantle-dominated magmas span the entire profile. One sample from RKZ and others from the western TMC have lower $Sr_i$ (~0·704) and higher $Nd_i$ isotopic values (~0·5127) (e.g. samples MM 40 and AVQ 221; dashed arrows in Fig. 12c and d), comparable with those from Valja Strz (VS 4, 12, 13), thus indicating that the source region in the mantle did not change between 82 and 71 Ma. Increasing $^{87}Sr/^{86}Sr_i$ ($\geq$0·706) and decreasing $^{143}Nd/^{144}Nd_i$, as low as 0·5124, probably indicate a longer residence time of the magma in the upper crust, contemporaneously with more crustal assimilation.

### Tectonic model

Calc-alkaline geochemical characteristics, including enrichment in LILE and depletion in HFSE, clearly point to a subduction-related origin for the Apuseni–Banat–Timok–Srednogorie (ABTS) magmatic belt. This Late Cretaceous belt was more linearly oriented (east–west) prior to Cenozoic deformation of its western segment northward, resulting in a NNW–SSE orientation (Fügenschuh & Schmid, 2005; Ustaszewski *et al.*, 2008; Fig. 1). Several broadly subduction-related tectonic models have been proposed to explain the evolution of the Cretaceous magmatic arc, including extensional rifting associated with

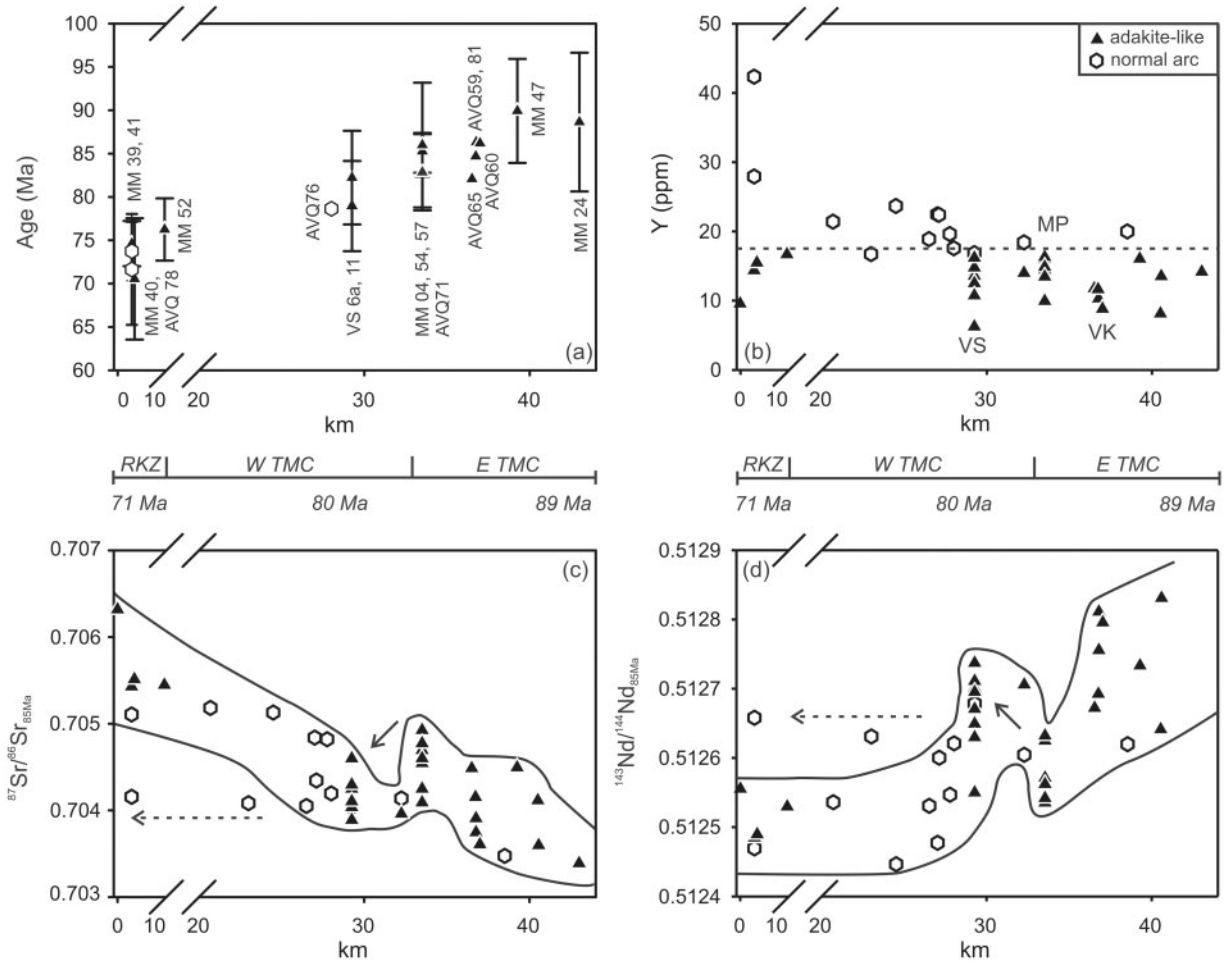


**Fig. 12.** Across-arc variations in age and isotopic composition from west (0 km = RKZ) to the east (43 km = TMC), projected onto a section line of WSW–ENE orientation. (a) U–Pb ages by LA-ICP-MS (this study; error bars are 2SD) and ID-TIMS (Peytcheva *et al.*, 2002; von Quadt *et al.*, 2002, 2003, 2007; errors within the symbol size). (b) Y vs distance. The dotted line separates the adakite-like (Y <18 ppm) from the normal arc field. (c) $^{87}Sr/^{86}Sr_i$ vs distance. (d) $^{143}Nd/^{144}Nd_i$ vs distance. Asthenospheric input is indicated by the continuous-line arrows. The dashed arrow indicates the minimally contaminated mantle source for the formation of the youngest magmas (AVQ 221, MM 40). VS, Valja Strz; MP, Majdanpek; VK, Veliki Krivelj.

orogenic collapse (Berza *et al.*, 1998; Bojar *et al.*, 1998; Willingshofer *et al.*, 2001; Iancu *et al.*, 2005), slab tear during or after subduction and continental collision (Neubauer, 2002), or rollback of a subducting oceanic slab (Lips, 2002; von Quadt *et al.*, 2005; Zimmerman *et al.*, 2008). The slab rollback model implies a gradual steepening of a northward subducting lithosphere slab, derived from the Jurassic to Cretaceous Vardar ocean. Rollback is generated by enhanced vertical gravitational force relative to the lateral tectonic force acting on a slab. It leads to upper plate extension, corner flow within the asthenosphere, and partial melting of the mantle wedge. Upper-crustal extension allows mantle-derived melts to access higher crustal levels. Slab rollback can occur during normal subduction of oceanic lithosphere, or during and even after continental collision, thereby enhancing orogenic collapse (see Berza *et al.*, 1998; Neubauer, 2002).

Our new data on the Late Cretaceous magmatism in Serbia can best be explained by a slab rollback model. Continuous sediment accretion in the forearc, combined with slab rollback, led to the observed age progression from ENE to WSW (Figs 12a and 13), or originally from north to south in the Late Cretaceous (i.e. before arc bending). Mantle-like isotopic values for the early primitive samples in the easternmost TMC imply that magmas were produced within the mantle wedge above the subduction zone, with minimal melting of crustal rocks but variable lower-crustal amphibole fractionation (Fig. 13a). Asthenospheric input, particularly prominent at Valja Strz further west between 82 and 78 Ma, indicates that extensional conditions were initiated by the rollback (Fig. 13b). Widespread deposition of volcanoclastic sediments produced by extension in the upper crust during this phase of volcanism (Karamata *et al.*, 1997) is also

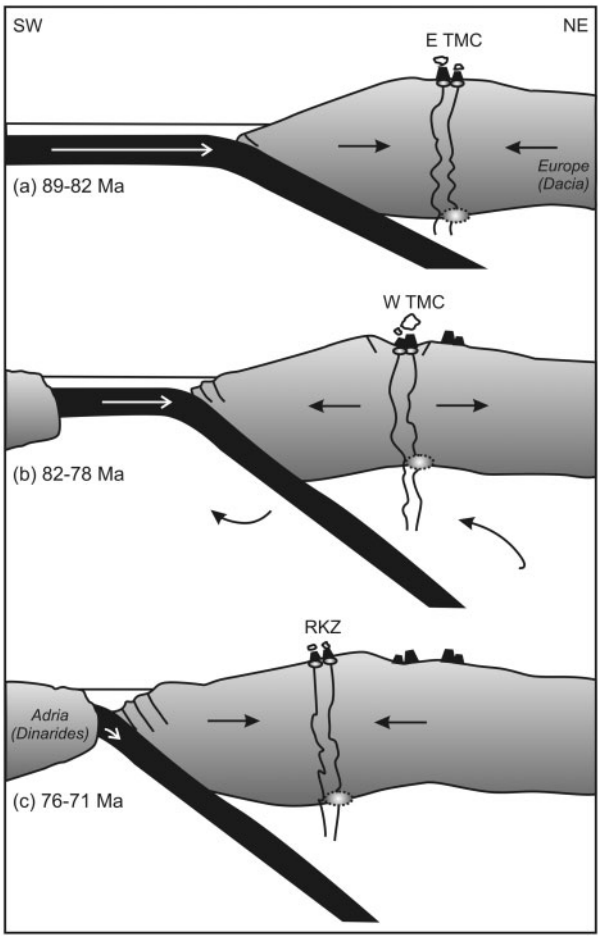


**Fig. 13.** Schematic tectonic model for the evolution of the TMC and RKZ (not to scale). (a) Initial situation along the eastern active margin of the TMC with subduction of the Vardar Ocean since the Early Cretaceous (Schmid *et al.*, 2008). (b) Initiation of the slab rollback leads to extension in the upper crust and asthenosphere flowing into the mantle wedge, producing more depleted Sr and Nd isotope compositions. (c) Arrival of the Adriatic continental fragment leads to compression in the upper crust, thus increasing the magma residence time in the magma chambers, favoring a greater degree of assimilation of magmas from the same source region in the mantle wedge. High-pressure amphibole fractionation in lower-crustal magma chambers (dashed magma chamber) producing the adakite-like trend takes place during all three tectonic phases.

consistent with this model. Continuous slab rollback would lead to increased asthenospheric input, and consequently decreased $^{87}Sr/^{86}Sr_i$ and increased $^{143}Nd/^{144}Nd_i$, as observed. Asthenospheric input is apparent even in some young samples (MM 40, AVQ 221) located in the west, but increasingly radiogenic $^{87}Sr/^{86}Sr_i$ and $^{143}Nd/^{144}Nd_i$ compositions suggest a general increase in crustal assimilation towards the western TMC and the RKZ. Longer crustal magma residence times seem to provide the best explanation for this phenomenon, perhaps related to the onset of collision and more compressive conditions along the arc. Termination of calc-alkaline magmatism at ~71 Ma probably reflects final closure of the Vardar ocean in this arc segment and stalling of the subducting slab as a result of collision of the Adriatic block (Fig. 13c). A return to continental collision is confirmed by tectonostratigraphic evidence for renewed thrusting in the Getic basement units in the Late Maastrichtian (70–65 Ma; Iancu *et al.*, 2005) and subsequent orogenic shortening in the Dinarides further to the west.

## CONCLUSIONS

The Timok and Ridanj–Krepoljin segments of a Late Cretaceous magmatic arc in southeastern Europe show intimately related magmas that apparently follow a common trend of crustal contamination of a subduction-related mantle melt. This contrasts with a more complex variation in trace-element signatures, including variable degrees of alkali enrichment and normal arc-like, as well as adakite-like, Sr–Y–REE differentiation trends. Systematic regional variations in age and geochemical signatures, especially in the degree of crustal contamination, indicate an evolving geodynamic setting related to slab rollback and ultimate continental collision. Despite this complexity, the trace-element and isotope geochemistry can be quantitatively modeled by a rather simple combination of lower-crustal hydrous fractionation of abundant high-pressure amphibole along with upper-crustal fractionation and assimilation involving abundant plagioclase crystallization. The association of the largest porphyry-copper and high-sulfidation epithermal Cu–Au deposits with some of the adakite-like magmas can be linked to volatile-rich magmas.

This study illustrates the value of energy-constrained assimilation and fractional crystallization modeling when trace-element, isotopic, and geochronological data are combined. Further testing of our interpretations might include more detailed study of sequential normal arc and adakite-like intrusions in single magmatic centers where both occur together. Studies of melt inclusions and phenocryst compositions would help to incorporate major-element variations in a full petrological model for fractional crystallization and assimilation of separately ascending magma batches. More detailed modeling should also consider the likely re-mixing of magmas with variable ascent paths, which probably contributes to so far unexplained scatter in our geochemical data.

## ACKNOWLEDGEMENTS

We thank Stevan Velev for assistance with the field work. Avala Resources Ltd. (former DUNDEE Precious Metal Inc.) is thanked for providing access to borehole samples. The paper benefited from detailed reviews by S. Foley, V. Janousek and one anonymous reviewer.

## FUNDING

This study was funded by the Swiss National Science Foundation Projects Nos 20020-116693, 20020-124906/1 and 20020-135302/1, which is gratefully acknowledged.

## SUPPLEMENTARY DATA

Supplementary data for this paper are available at *Journal of Petrology* online.

## REFERENCES

Abratis, M. & Wörner, G. (2001). Ridge collision, slab-window formation, and the flux of Pacific asthenosphere into the Caribbean realm. *Geology* **29**, 127–130.

Alonso-Perez, R., Müntener, O. & Ulmer, P. (2009). Igneous garnet and amphibole fractionation in the roots of island arcs: experimental constraints on andesitic liquids. *Contributions to Mineralogy and Petrology* **157**, 542–558.

Atherton, M. P. & Petford, N. (1993). Generation of sodium-rich magmas from newly underplated basaltic crust. *Nature* **362**, 144–146.

Banjesevic, M. (2001). The volcanic rocks petrology and K–Ar ages for widen zone Bor ore deposit as part of the Timok magmatic complex (east Serbia). Geological Institute of Romania (ed.) *ABCD Geode Workshop*, Vata Bai, Romania. Bucarest: Geological Institute of Romania, pp. 39–40.

Banjesevic, M., Cvetkovic, V., Kozelj, D., Peytcheva, I. & von Quadt, A. (2002). Timok magmatic complex and Ridanj–Krepoljin zone: geodynamic evolution. In: Kozelj, D. & Jelenkovic, R. (eds) *100 Years Copper Institute of Bor*. Bor, Serbia: RTB Bor Holding Company, pp. 199–202.

Banjesevic, M., Cvetkovic, V., von Quadt, A., Peytcheva, I. & Cocic, S. (2006). Geodynamic reconstructions based of the magmatism in the Timok magmatic complex (east Serbia)—part of the Carpathian–Balkan belt. In: Sudar, M., Ercegovac, M. & Grubic, A. (eds) *XVII Congress CBGA*. Belgrade: Serbian Geological Society, pp. 27–29.

Berza, T., Constantinescu, E. & Vlad, S. N. (1998). Upper Cretaceous magmatic series and associated mineralisation in the Carpathian–Balkan orogen. *Resource Geology* **48**, 291–306.

Bohrson, W. A. & Spera, F. J. (2001). Energy-constrained open-system magmatic processes II: Application of energy-constrained assimilation–fractional crystallization (EC-AFC) model to magmatic systems. *Journal of Petrology* **42**, 1019–1041.

Bojar, A. V., Neubauer, F. & Fritz, H. (1998). Cretaceous to Cenozoic thermal evolution of the southwestern South Carpathians: evidence from fission-track thermochronology. *Tectonophysics* **297**, 229–249.

Bottazzi, P., Tiepolo, M., Vannucci, R., Zanetti, A., Brumm, R., Foley, S. F. & Oberti, R. (1999). Distinct site preferences for heavy and light REE in amphibole and the prediction of *D*-Amph/L(REE). *Contributions to Mineralogy and Petrology* **137**, 36–45.

Bourdon, E., Eissen, J. P., Monzier, M., Robin, C., Martin, H., Cotten, J. & Hall, M. L. (2002). Adakite-like lavas from Antisana volcano (Ecuador): Evidence for slab melt metasomatism beneath the Andean Northern Volcanic Zone. *Journal of Petrology* **43**, 199–217.

Burnham, C. W. (1979). The importance of volatile constituents. In: Yoder, H. S. J. (ed.) *The Evolution of the Igneous Rocks: Fiftieth Anniversary Perspectives*. Princeton, NJ: Princeton University Press, pp. 439–482.

Castillo, P. R., Janney, P. E. & Solidum, R. U. (1999). Petrology and geochemistry of Camiguin Island, southern Philippines: insights to the source of adakites and other lavas in a complex arc setting. *Contributions to Mineralogy and Petrology* **134**, 33–51.

Chambefort, I., Moritz, R. & von Quadt, A. (2007). Petrology, geochemistry and U–Pb geochronology of magmatic rocks from the high-sulfidation epithermal Au–Cu Chelopech deposit, Srednogorie zone, Bulgaria. *Mineralium Deposita* **42**, 665–690.

Chiaradia, M. (2009). Adakite-like magmas from fractional crystallization and melting–assimilation of mafic lower crust (Eocene Macuchi arc, Western Cordillera, Ecuador). *Chemical Geology* **265**, 468–487.

Chiaradia, M., Müntener, O., Beate, B. & Fontignie, D. (2009). Adakite-like volcanism of Ecuador: lower crust magmatic evolution and recycling. *Contributions to Mineralogy and Petrology* **158**, 563–588.

Chung, S. L., Liu, D. Y., Ji, J. Q., Chu, M. F., Lee, H. Y., Wen, D. J., Lo, C. H., Lee, T. Y., Qian, Q. & Zhang, Q. (2003). Adakites from continental collision zones: melting of thickened lower crust beneath southern Tibet. *Geology* **31**, 1021–1024.

Ciobanu, C., Cook, N. & Stein, H. (2002). Regional setting and geochronology of the Late Cretaceous banatitic magmatic and metallogenetic belt. *Mineralium Deposita* **37**, 541–567.

Clark, A. H. & Ullrich, T. D. (2004). $^{40}$Ar–$^{39}$Ar age data for andesitic magmatism and hydrothermal activity in the Timok massif, eastern Serbia: implications for metallogenic relationships in the Bor copper gold subprovince. *Mineralium Deposita* **39**, 256–262.

Davidson, J., Turner, S., Handley, H., Macpherson, C. & Dosseto, A. (2007). Amphibole 'sponge' in arc crust? *Geology* **35**, 787–790.

Defant, M. J. & Drummond, M. S. (1990). Derivation of some modern arc magmas by melting of young subducted lithosphere. *Nature* **347**, 662–665.

Defant, M. J. & Kepezhinskas, P. (2001). Adakites: A review of slab melting over the past decade and the case for a slab-melt component in arcs. *EOS Transactions American Geophysical Union* **82**, 68–69.

de Jonge, M. R., Wortel, M. J. R. & Spakman, W. (1994). Regional-scale tectonic evolution and the seismic velocity structure of the lithosphere and upper-mantle—the Mediterranean region. *Journal of Geophysical Research—Solid Earth* **99(B6)**, 12091–12108.

DePaolo, D. J. (1981). Trace-element and isotopic effects of combined wallrock assimilation and fractional crystallization. *Earth and Planetary Science Letters* **53**, 189–202.

Downes, H., Seghedi, I., Szakacs, A., Dobosi, G., James, D. E., Vaselli, O., Rigby, I. J., Ingram, G. A., Rex, D. & Pecskay, Z. (1995). Petrology and geochemistry of Late Tertiary–Quaternary mafic alkaline volcanism in Romania. *Lithos* **35**, 65–81.

Drummond, M. S., Defant, M. J. & Kepezhinskas, P. K. (1996). Petrogenesis of slab-derived trondhjemitetonalitedacite/adakite magmas. *Transactions of the Royal Society of Edinburgh: Earth Sciences* **87**, 205–215.

Duchesne, J. C., Liegeois, J. P., Iancu, V., Berza, T., Matukov, D. I., Tatu, M. & Sergeev, S. A. (2008). Post-collisional melting of crustal sources: constraints from geochronology, petrology and Sr, Nd isotope geochemistry of the Variscan Sichevita and Poniasca granitoid plutons (South Carpathians, Romania). *International Journal of Earth Sciences* **97**, 705–723.

Dupont, A., Vander Auwera, J., Pin, C., Marincea, S. & Berza, T. (2002). Trace element and isotope (Sr, Nd) geochemistry of porphyry- and skarn-mineralising Late Cretaceous intrusions from Banat, western South Carpathians, Romania. *Mineralium Deposita* **37**, 568–586.

Fügenschuh, B. & Schmid, S. M. (2005). Age and significance of core complex formation in a very curved orogen: evidence from fission track studies in the South Carpathians. *Tectonophysics* **404**, 33–53.

Georgiev, S. (2008). Sources and evolution of Late Cretaceous magmatism in Eastern Srednogorie, Bulgaria: constraints from petrology, isotope geochemistry and geochronology, PhD thesis, ETH Zurich.

Georgiev, S., Marchev, P., Heinrich, C. A., von Quadt, A., Peytcheva, I. & Manetti, P. (2009). Origin of nepheline-normative high-K ankaramites and the evolution of eastern Srednogorie arc in SE Europe. *Journal of Petrology* **50**, 1899–1933.

Ghiorso, M. S. & Sack, R. O. (1995). Chemical mass transfer in magmatic processes IV. A revised and internally consistent thermodynamic model for the interpolation and extrapolation of liquid–solid equilibria in magmatic systems at elevated temperatures and pressures. *Contributions to Mineralogy and Petrology* **119**, 197–212.

Guillong, M., Meier, D. L., Allan, M. M., Heinrich, C. A. & Yardley, B. W. D. (2008). SILLS: a Matlab-based program for the reduction of laser ablation ICP-MS data of homogeneous materials and inclusions. In: Sylvester, P. (ed.) *Laser-Ablation-ICP-MS in the Earth Sciences, Current Practices and Outstanding Issues. Mineralogical Association of Canada, Short Course* **29**, 328–333.

Günther, D., von Quadt, A., Wirz, R., Cousin, H. & Dietrich, V. J. (2001). Elemental analyses using laser ablation-inductively coupled plasma-mass spectrometry (LA-ICP-MS) of geological samples fused with $Li_2B_4O_7$ and calibrated without matrix-matched standards. *Mikrochimica Acta* **136**, 101–107.

Gutscher, M.-A., Maury, R., Eissen, J.-P. & Bourdon, E. (2000). Can slab melting be caused by flat subduction? *Geology* **28**, 535–538.

Hedenquist, J. W. & Lowenstern, J. B. (1994). The role of magmas in the formation of hydrothermal ore deposits. *Nature* **370**, 519–527.

Hofmann, A. W. (1988). Chemical differentiation of the Earth—the relationship between mantle, continental crust, and oceanic crust. *Earth and Planetary Science Letters* **90**, 297–314.

Hora, J. M., Singer, B. S., Wörner, G., Beard, B., Jicha, B. R. & Johnson, C. (2009). Shallow and deep crustal control on differentiation of calc-alkaline and tholeiitic magma. *Earth and Planetary Science Letters* **285**, 75–86.

Iancu, V., Berza, T., Seghedi, I., Gheuca, I. & Hann, H. P. (2005). Alpine polyphase tectono-metamorphic evolution of the South Carpathians: a new overview. *Tectonophysics* **410**, 337–365.

Jackson, S., Pearson, N., Griffin, W. & Belousova, E. (2004). The application of laser ablation-inductively coupled plasma-mass spectrometry to *in situ* U–Pb zircon geochronology. *Chemical Geology* **211**, 47–69.

Jankovic, S. (1997). The Carpatho-Balkanides and adjacent area: A sector of the Tethyan Eurasian metallogenic belt. *Mineralium Deposita* **32**, 426–433.

Jankovic, S., Jovanovic, M., Karamata, S. & Lovric, A. (1981). Isotopic age of some rocks from the Timok eruptive area. *Academy of Serbian Science and Arts, Natural Science and Mathematics* **48**, 87–94.

Jego, S., Maury, R. C., Polve, M., Yumul, G. P., Bellon, H., Tamayo, R. A. & Cotten, J. (2005). Geochemistry of adakites from the Philippines: Constraints on their origins. *Resource Geology* **55**, 163–187.

Karamata, S. & Krstic, B. (1996). Terranes of Serbia and neighbouring areas. In: Knezevic, V., Dordjevic, V. & Krstic, B. (eds) *Terranes of Serbia*. Belgrade: University of Belgrade and Serbian Acadamy of Sciences and Art, pp. 25–40.

Karamata, S., Knezevic, V., Pecskay, Z. & Djordjevic, M. (1997). Magmatism and metallogeny of the Ridanj–Krepoljin belt (eastern Serbia) and their correlation with northern and eastern analogues. *Mineralium Deposita* **32**, 452–458.

Kay, R. W. (1978). Aleutian magnesian andesites: melts from subducted Pacific ocean crust. *Journal of Volcanology and Geothermal Research* **4**, 117–132.

Kay, R.W. & Kay, S. M. (2002). Andean adakites: three ways to make them. *Acta Petrologica Sinica* **18**, 303–311.

Kay, R. W., Ramos, V. A. & Marquez, Y. M. (1993). Evidence in Cerro Pampa volcanic rocks for slab-melting prior to ridge–trench collision in southern South America. *Journal of Geology* **101**, 703–714.

Kay, S. M., Mpodozis, C., Ramos, V. A. & Munizaga, F. (1991). Magma source variations for mid–late Tertiary magmatic rocks associated with a shallowing subduction zone and thickening crust in the central Andes (28–33°S). In: Harmon, R. S. & Rapela, C. (eds) *Andean Magmatism and its Tectonic Setting. Geological Society of America, Special Papers* **265**, 113–137.

Klein, E. M. (2003). Geochemistry of the igneous oceanic crust. In: Turekian, K. K. & Holland, H. D. (eds) *Treatise on Geochemistry*. Amsterdam: Elsevier, pp. 433–459.

Kouzmanov, K., Moritz, R., von Quadt, A., Chiaradia, M., Peytcheva, I., Fontignie, D., Ramboz, C. & Bogdanov, K. (2009). Late Cretaceous porphyry Cu–Au association in the southern Panagyurishte district, Bulgaria: the paired Vlaykov Vruh and Elshitsa deposit. *Mineralium Deposita* **44**, 611–646.

Kräutner, H. G. & Krstic, B. (2003). Geological map of the Carpatho-Balkanides between Mehadia, Oravita, Nis and Sofia. In: *18th Congress of the Carpathian–Balkan Geological Association, Belgrade*. Beograd: Geoinstitut.

Krstic, B. (2001). Timing of the Neogene geotectonic events in the Carpatho-Balkanidic and Dinaridic Alps with adjoining regions. In: *PANCARDI 2001, Sopron*, 25 p.

Le Bas, M. J., Le Maitre, R. W., Streckeisen, A. & Zanettin, B. (1986). A chemical classification of volcanic rocks based on the total alkali–silica diagram. *Journal of Petrology* **27**, 745–750.

Liegeois, J. P., Berza, T., Tatu, M. & Duchesne, J. C. (1996). The Neoproterozoic Pan-African basement from the Alpine lower Danubian nappe system (South Carpathians, Romania). *Precambrian Research* **80**, 281–301.

Lips, A. (2002). Correlating magmatic–hydrothermal ore deposit formation over time with geodynamic processes in SE Europe. In: Blundell, D. J., Neubauer, F. & von Quadt, A. (eds) *The Timing and Location of Major Ore Deposits in an Evolving Orogen. Geological Society, London, Special Publications* **204**, 69–79.

Ludwig, K. J. (2003). *Isoplot 3.00. Berkeley Geochronology Center, Special Publications* **70**.

Macpherson, C., Dreher, S. & Thirlwall, M. (2006). Adakites without slab melting: High pressure differentiation of island arc magma, Mindanao, the Philippines. *Earth and Planetary Science Letters* **243**, 581–593.

Maksimov, A. P. (2009). The influence of water on the temperature of amphibole stability in melts. *Journal of Volcanology and Seismology* **3**, 27–33.

Marovic, M., Djokovic, I. & Toljic, M. (1998). Genesis of the neotectonic structures of Serbia. *Annales Géologiques de la Peninsule Balkanique* **62**, 25–45.

Martin, H. (1987). Evolution in composition of granitic rocks controlled by time-dependent changes in petrogenetic processes—examples from the Archean of Eastern Finland. *Precambrian Research* **35**, 257–276.

Mitchell, A. H. G. (1996). Distribution and genesis of some epizonal Zn–Pb and Au provinces in the Carpathia–Balkan region. *Transactions of the Institution of Mining and Metallurgy, Section B* **105**, 127–138.

Moore, G. & Carmichael, I. S. E. (1998). The hydrous phase equilibria (to 3 kbar) of an andesite and basaltic andesite from western Mexico: constraints on water content and conditions of phenocryst growth. *Contributions to Mineralogy and Petrology* **130**, 304–319.

Neubauer, F. (2002). Contrasting Late Cretaceous with Neogene ore provinces in the Alpine–Balkan–Carpathian–Dinaride collision belt. In: Blundell, D. J., Neubauer, F. & von Quadt, A. (eds) *The Timing and Location of Major Ore Deposits in an Evolving Orogen. Geological Society, London, Special Publications* **204**, 90–100.

Oyarzun, R., Marquez, A., Lillo, J., Lopez, I. & Rivera, S. (2001). Giant versus small porphyry copper deposits of Cenozoic age in Northern Cile: adakite versus normal calc-alkaline magmatism. *Mineralium Deposita* **36**, 794–798.

Patrascu, S., Panaiotu, C., Seclaman, M. & Panaiotu, B. (1994). Timing of rotational motion of Apuseni Mountains (Romania): paleomagnetic data from Tertiary magmatic rocks. *Tectonophysics* **233**, 163–176.

Peccerillo, A. & Taylor, S. R. (1976). Geochemistry of Eocene calc-alkaline volcanic rocks from the Kastamonu area, Northern Turkey. *Contributions to Mineralogy and Petrology* **58**, 63–81.

Pecskay, Z., Djordevic, M., Karamata, S. & Knezevic, V. (1992). , Prvi podaci o izotopskoj starosti vulkanskih stena Ridanjsko-krepoljinske zone (istocna Srbija). (First data on the age of the volcanic rocks from the Ridanj–Krepoljin zone.) Zapisnici SGD (in press).

Petford, N. & Gallagher, K. (2001). Partial melting of mafic (amphibolitic) lower crust by periodic influx of basaltic magma. *Earth and Planetary Science Letters* **193**, 493–499.

Peytcheva, I., von Quadt, A., Cvetkovic, V., Kozelj, D. & Banjesevic, M. (2002). Geochronology, geochemistry and isotope tracing of the Cretaceous magmatism of eastern Serbia as part of the Apuseni–Timok–Srednogorie metallogenic belt. *Geologica Carpathia* **53**, 175–177.

Pin, C., Briot, D., Bassin, C. & Poitrasson, F. (1994). Concomitant separation of strontium and samarium–neodymium for isotopic analysis in silicate samples, based on specific extraction chromatography. *Analytica Chimica Acta* **298**, 209–217.

Popov, P. N. (1981). Magmotectonic features of the Banat–Srednogorie belt. *Geologica Balcanica* **11**, 43–72.

Popov, P. N., Berza, T., Grubic, A. & Ioane, D. (2002). Late Cretaceous Apuseni–Banat–Timok–Srednogorie (ABTS) magmatic and metallogenic belt in the Carpathian–Balkan orogen. *Geologica Balcanica* **32**, 145–163.

Rabbia, O. M., Hernandez, L. B., King, R. W. & Lopez-Escobar, L. (2002). Discussion on 'Giant versus small porphyry copper deposits of Cenozoic age in Northern Cile: adakite versus normal calc-alkaline magmatism' by Oyarzun *et al*. *Mineralium Deposita* **37**, 791–794.

Richards, J. P. (2002). Discussion on 'Giant versus small porphyry copper deposits of Cenozoic age in Northern Cile: adakite versus normal calc-alkaline magmatism' by Oyarzun *et al*. *Mineralium Deposita* **37**, 788–790.

Richards, J. P. & Kerrich, R. (2007). Special paper: Adakite-like rocks: Their diverse origins and questionable role in metallogenesis. *Economic Geology* **102**, 537–576.

Rohrlach, B. D. & Loucks, R. R. (2005). Multi-million-year cycling ramp-up of volatiles in a lower crustal magma chamber reservoir trapped below the Tampakan copper–gold deposit by Mio-Pliocene crustal compression in the southern Philippines. In: Porter, T. M. (ed.) *Super Porphyry Copper and Gold Deposits: A Global Perspective*. Adelaide: PGC Publishing, 270 p.

Schmid, S. M., Bernoulli, D., Fügenschuh, B., Matenco, L., Schefer, S., Schuster, R., Tischler, M. & Ustaszewski, K. (2008). The Alpine–Carpathian–Dinaridic orogenic system: correlation and evolution of tectonic units. *Swiss Journal of Geosciences* **101**, 139–183.

Singer, B. S., Jicha, B. R., Leeman, W. P., Rogers, N. W., Thirlwall, M. F., Ryan, J. & Nicolaysen, K. E. (2007). Along-strike trace element and isotopic variation in Aleutian island arc basalt: Subduction melts sediments and dehydrates serpentine. *Journal of Geophysical Research* **112**, doi:10.1029/2006JB004897.

Spera, F. J. & Bohrson, W. A. (2001). Energy-constrained open-system magmatic processes I: General model and energy-constrained assimilation and fractional crystallization (EC-AFC) formulation. *Journal of Petrology* **42**, 999–1018.

Stoykov, S., Peytcheva, I., von Quadt, A., Moritz, R., Frank, M. & Fontignie, D. (2004). Timing and magma evolution of the Chelopech volcanic complex (Bulgaria). *Schweizerische Mineralogische und Petrographische Mitteilungen* **84**, 101–117.

Stracke, A., Bizimis, M. & Salters, V. J. M. (2003). Recycling oceanic crust: quantitative constraints. *Geochemistry, Geophysics, Geosystems* **4**, 8003, doi:10.1029/2001GC000223.

Streckeisen, A. (1976). To each plutonic rock its proper name. *Earth-Science Reviews* **12**, 1–33.

Sun, S. & McDonough, (1989). Chemical and isotopic systematics of oceanic basalts: implications for mantle composition and processes. In: Saunders, A. D. & Norry, M. J. (eds) *Magmatism in the Ocean Basins. Geological Society, London, Special Publications* **42**, 313–345.

Ulmer, P. (1988). High-pressure phase equilibria of a calc-alkaline picro-basalt: implications for the genesis of calc-alkaline magmas. *Carnegie Institution of Washington Geophysical Laboratory Annual Report* 28–35.

Ustaszewski, K., Schmid, S. M., Fügenschuh, B., Tischler, M., Kissling, E. & Spakman, W. (2008). A map view restoration of the Alpine–Carpathian–Dinaridic system for the Early Miocene. *Swiss Journal of Geoscience* **101**, S273–S294.

von Quadt, A., Ivanov, Z. & Peytcheva, I. (2001). The Central Srednogorie (Bulgaria) part of the Cu (Au–Mo) belt of Europe: A review of the geochronological data and the geodynamical models in the light of the new structural and isotopic studies. In: Piestrzynski, A. (ed.) *Mineral Deposits at the Beginning of the 21st Century, Proceedings of the Joint Sixth Biennial SGA–SEG Meeting, Krakow*. Tokyo: A.A. Balkema Publishers, pp. 555–558.

von Quadt, A., Peytcheva, I., Cvetkovic, V., Banjesevic, M. & Kozelj, D. (2002). Geochronology, geochemistry and isotope tracing of the Cretaceous magmatism of east Serbia as part of the Apuseni–Timok–Srednogorie metallogenic belt. *Geologica Carpathia* **53**, 175–177.

von Quadt, A., Peytcheva, I. & Cvetkovic, V. (2003). Geochronology, geochemistry and isotope tracing of the Cretaceous magmatism of East Serbia and Panagyurishte district (Bulgaria) as part of the Apuseni–Timok–Srednogorie metallogenic belt in Eastern Europe. In: Eliopoulos, D. E. *et al*., (eds) *The Seventh Biennial SGA Meeting, Athens*. Rotterdam: Millpress, pp. 407–410.

von Quadt, A., Moritz, R., Peytcheva, I. & Heinrich, C. (2005). Geochronology and geodynamics of Late Cretaceous magmatism and Cu–Au mineralization in the Panagyurishte region of the Apuseni–Banat–Timok–Srednogorie belt, Bulgaria. *Ore Geology Reviews* **27**, 95–126.

von Quadt, A., Peytcheva, I. & Heinrich, C. (2007). Upper Cretaceous magmatic evolution and related Cu–Au mineralization in Bulgaria and Serbia. In: Andrew, C. J. (ed.) *Ninth Biennial Meeting of the Society for Geology Applied to Mineral Deposits SGA, Dublin*. Dublin: Irish Association for Economic Geology, pp. 861–864.

von Quadt, A., Erni, M., Martinek, K., Moll, M., Peytcheva, I. & Heinrich, C. A. (2011). Zircon crystallization and the lifetimes of ore-forming magmatic–hydrothermal systems. *Geology* **39**, 731–734.

Wang, Q., Xu, J. F., Jian, P., Bao, Z. W., Zhao, Z. H., Li, C. F., Xiong, X. L. & Ma, J. L. (2006). Petrogenesis of adakitic porphyries in an extensional tectonic setting, Dexing, South China: Implications for the genesis of porphyry copper mineralization. *Journal of Petrology* **47**, 119–144.

Willingshofer, E., Andriessen, P., Cloetingh, S. & Neubauer, F. (2001). Detrital fission track thermochronology of Upper Cretaceous syn-orogenic sediments in the South Carpathians (Romania): inferences on the tectonic evolution of a collisional hinterland. *Basin Research* **13**, 379–395.

Wilson, M. & Bianchini, G. (1999). Tertiary–Quaternary magmatism within the Mediterranean and surrounding regions. In: Durand, B., Jolivet, L., Horvath, F. & Séranne, M. (eds) *The Mediterranean Basins: Tertiary Extension within the Alpine Orogen. Geological Society, London, Special Publications* **156**, 141–168.

Yogodzinski, G. M., Kay, R. W., Volynets, O. N., Koloskov, A. V. & Kay, S. M. (1995). Magnesian andesite in western Aleutian Komandorsky region: implications for slab melting and processes in the mantle wedge. *Geological Society of America Bulletin* **107**, 505–519.

Zhang, L. C., Xiao, W. J., Qin, K. Z. & Zhang, Q. (2006). The adakite connection of the Tuwu–Yandong copper porphyry belt, eastern Tianshan, NW China: trace element and Sr–Nd–Pb isotope geochemistry. *Mineralium Deposita* **41**, 188–200.

Zimmerman, A., Stein, H. J., Hannah, J. L., Kozelj, D., Bogdanov, K. & Berza, T. (2008). Tectonic configuration of the Apuseni–Banat–Timok–Srednogorie belt, Balkans–South Carpathians, constrained by high precision Re–Os molybdenite ages. *Mineralium Deposita* **43**, 1–21.